Compressive Sensing Assisted Generalized Quadrature Spatial Modulation for Massive MIMO systems

Lixia Xiao, Pei Xiao, *Senior Member, IEEE*, Yue Xiao, *Member, IEEE*, Harald Haas, Abdelrahim Mohamed, and Lajos Hanzo, *Fellow, IEEE*

***Abstract*—A novel Multiple-Input and Multiple-Output (MIMO) transmission scheme termed as Generalized Quadrature Spatial Modulation (G-QSM) is proposed. It amalgamates the concept of Quadrature Spatial Modulation (QSM) and spatial multiplexing for the sake of achieving a high throughput, despite relying on low number of Radio Frequency (RF) chains. In the proposed G-QSM scheme, the conventional constellation points of the spatial multiplexing structure are replaced by the QSM symbols, hence the information bits are conveyed both by the antenna indices as well as by the classic Amplitude/Phase Modulated (APM) constellation points. The upper bounds of the Average Bit Error Probability (ABEP) of the proposed G-QSM system in high throughput massive MIMO configurations are derived. Furthermore, an Efficient Multipath Orthogonal Matching Pursuit (EM-OMP) based Compressive Sensing (CS) detector is developed for our proposed G-QSM system. Both our analytical and simulation results demonstrated that the proposed scheme is capable of providing considerable performance gains over the existing schemes in massive MIMO configurations.**

***Index Terms*—Quadrature Spatial Modulation (QSM), Multiple-Input Multiple-Output (MIMO), Vertical Bell Labs Space-Time (VBLAST).**

Introduction

MASSIVE Multi-input Multi-output (MIMO) [1]-[4] systems are capable of significantly increasing the transmission rate, reliability and system capacity by employing numerous antennas. Hence they may be deemed a key technology in next-generation wireless system. In massive MIMO systems, the classic Vertical Bell Laboratories Space Time (V-BLAST) based MIMO schemes [5]-[6] require numerous Radio Frequency (RF) chains, hence imposing substantial implementation cost and signal processing complexity. As a result, how to design a large-scale MIMO scheme to strike an elegant tradeoff between the throughput and implementation cost has attracted a lot attention.

Recently, Spatial Modulation based variants, which employ the activated antenna indices as an additional means of implicitly conveying information, have been advocated as novel low-cost RF chain based MIMO transmission structures. To be more specific, in SM [7], one out of N_t Transmit Antennas (TAs) is activated to implicitly convey information. Due to the advantages of the single RF chain based MIMO structure, SM scheme has also been studied in massive MIMO communication scenarios [8]-[11]. However, the low number of RF chains limits the transmission rate of the SM scheme. In order to increase its throughput, multiple activated TA based SM variants were proposed in [12]-[19]. Specifically, in the Generalized SM (GSM) scheme [12]-[15], N_u out of N_t TAs are activated to transmit different symbols, so that the transmission rate is significantly increased. In [16]-[17], the number of activated TAs ranged from one to N_t. Additionally, GSM combined with Space Time Block Coding (STBC) structures was designed in [18]-[19]. However, the above SM variants have the common feature that the information bits are conveyed both by the active TA index as well as by the Amplitude Phase Modulation (APM) symbols. In high-throughput massive MIMO scenarios, the number of information bits carried by the index is high, which makes the bit-to-symbol mapping and symbol-to-bit demapping challenging [20].

In order to address the mapping issues in SM based massive MIMO systems, a novel spatial multiplexing based SM scheme is proposed in [20], where the N_t TAs are partitioned into L groups and SM is employed in each group. We refer to this scheme as SM-VBLAST. Compared to the classic VBLAST system, an SM symbol instead

L. Xiao, P. Xiao, and A. Mohamed are with the school of Electrical Electronic Engineering of University of Surrey, GU1 7XH.

L. Xiao is also with the Wuhan National Laboratory for Optoelectronics, School of Electronic Information and Communications, Huazhong University of Science and Technology.

Y. Xiao, is with the National Key Laboratory of Science and Technology on Communications, University of Electronic Science and Technology of China 611731, Sichuan, China.

H. Hass is with Electronics and Electrical Engineering, University of Edinburgh.

L. Hanzo are with the school of Electronics and Computer Science, University of Southampton, Southampton SO17 1BJ, U.K. (email: lh@ecs.soton.ac.uk).

This work was supported in part by the U.K. Engineering and Physical Sciences Research Council under Grant EP/P03456X/1. The authors also would like to acknowledge the support of the University of Surrey 5GIC (http://www.surrey.ac.uk/5gic) members for the work.

L. Hanzo would like to acknowledge the financial support of the Engineering and Physical Sciences Research Council projects EP/Noo4558/1, EP/PO34284/1, COALESCE, of the Royal Society's Global Challenges Research Fund Grant as well as of the European Research Council's Advanced Fellow Grant QuantCom.

of a single AMP symbol is mapped to each group, so that the throughput is significantly increased at the same number of RF chains. As a result, the SM-VBLAST system circumvents the mapping issues in massive MIMO systems. Moreover, this SM-VBLAST scheme is capable of outperforming the conventional GSM scheme, despite its lower complexity, providing a 6 dB Signal to Noise Ratio (SNR) gain over the V-BLAST system having the same number of RF chains and the same throughput. However, how to fully exploit the advantages of index modulation in massive MIMO systems is still an open question to be investigated.

As an SM variants, Quadrature SM (QSM) [21] also constitutes a high-efficiency MIMO technique, which exploits both the in-phase and quadrature dimensions for enhancing the overall throughput of the conventional SM system. In the QSM scheme, both the indices of the real part as well as of the imaginary part of an M-ary APM symbol and the APM symbol itself convey information, hence resulting in higher throughput than conventional SM. Furthermore, the inter-antenna interference can also be avoided by the QSM scheme, since orthogonal symbols are transmitted by the activated antennas. Recently, the QSM design efforts have been mainly focused on its performance analysis [22]-[24], on its coherent vs non-coherent detection [25]-[27], as well as on practical communication systems [29]-[31]. To the best of our knowledge, QSM based high throughput MIMO schemes have not been investigated. On the other hand, since the SM based MIMO schemes exhibit an inherent transmit symbol sparsity, Compressive Sensing (CS) has been invoked as an efficient technique of detecting the SM based MIMO symbols [32]-[39].

Against the above background, the contributions of this paper are summarized as follows:

1) A novel low-complexity high throughput MIMO scheme namely Generalized Quadrature Spatial-Modulation (G-QSM) is proposed. The throughput achieved by the G-QSM system is analyzed and the optimal highest-throughput mapping is derived.
2) The upper bound of the Average Bit Error Probability (ABEP) of the proposed G-QSM system in high-throughput massive MIMO configurations is derived, where the optimal detector becomes impractical. Hence, the proposed upper bound of ABEP is helpful for performance evaluation in hight-throughput communication scenarios.
3) Furthermore, an Efficient Multipath Orthogonal Matching Pursuit (EM-OMP) based CS detector is proposed for our G-QSM system. Both our theoretical and simulation results demonstrated that the proposed G-QSM scheme employing a large number of TAs is capable of providing a 20 dB Signal to Noise Ratio (SNR) gain over the V-BLAST system having the same limited number of RF chains and the same throughput.

The remainder of this paper is organized as follows. Section II provides a rudimentary review of the conventional QSM system. In Section III, the system model, the rate achieved and the mapping methods employed in our proposed G-QSM system are introduced . In Section IV, the theoretical analysis of the G-QSM systems having massive MIMO configurations is presented. In Section V, the EM-OMP detector is proposed for our G-QSM system. Section VI portrays our simulation results. Finally, Section VII concludes this paper.

Notation: $\|\cdot\|$ denotes the Frobenious norms of a matrix. $|\cdot|$ represents the magnitude of a complex quantity. $(\cdot)^T$ and $(\cdot)^H$ stand for the transpose and the Hermitian transpose of a vector/matrix, respectively. $A\backslash B$ denotes removing the set B from the set A. C_m^n denotes the binomial coefficient.

QSM System

We consider a QSM system having N_t TAs and N_r Receive Antennas (RAs) operating in flat Rayleigh fading channels. In a QSM scheme, the information bits are partitioned in two parts, $2\log_2(N_t)$ bits are used for conveying the active TA indices and $\log_2(M)$ bits mapped to an M-ary APM symbol x. To be specific, $\log_2(N_t)$ bits are assigned to select one TA for transmitting the real part of signal x and another $\log_2(N_t)$ bits are used to select an active TA to transmit the imaginary part of x. Based on the above mapping rule, the transmitted signal $\mathbf{x} \in \mathbb{C}^{N_t \times 1}$can be represented as

$$\mathbf{x} = \begin{cases} [\underbrace{0,...,0}_{l_\Re - 1}, x_\Re + jx_\Im, \underbrace{0,...,0}_{N_t - l_\Re}]^T, \text{ if } l_\Re = l_\Im, \\ [\underbrace{0,...,0}_{l_\Re - 1}, x_\Re, 0, ..., 0, jx_\Im, \underbrace{0,...,0}_{N_t - l_\Im}]^T, \text{ else}, \end{cases} \tag{1}$$

where $x_\Re$ and $x_\Im$ denote the real and imaginary parts of x, respectively, while $l_\Re = (1, ..., N_t)$ and $l_\Im = (1, ..., N_t)$ represent the corresponding active TA indices.

Proposed Generalized QSM System

In order to improve the throughput of the QSM systems, a low-complexity yet high-throughput generalized QSM scheme is proposed in this section. Considering a MIMO system having N_t TAs, N_r RAs, the N_t TAs are split into L groups and in each group a single QSM symbol is constructed. Considering $N_t = 4$, $L = 2$ and QPSK for example, the proposed generalized QSM symbol set $\mathbb{X}_4^2$ is constructed of two QSM symbols $[\mathbf{x}_1, \mathbf{x}_2]$ as seen in (2), where x_1 and x_2 are the constellation symbols.

Generalized System Model of G-QSM

The generalized system model of the proposed G-QSM is shown in Fig. 1. As seen from Fig. 1, the information bits of $R = \sum_{i=1}^{L} R_i$ are partitioned into L $(1 \le L \le N_t/2)$ groups and then the QSM mapping principle is employed for each group. Assuming that the i-th $(i = 1, ..., L)$ QSM symbol employs N_Q^i TAs and M_i APM symbols, the i-th block

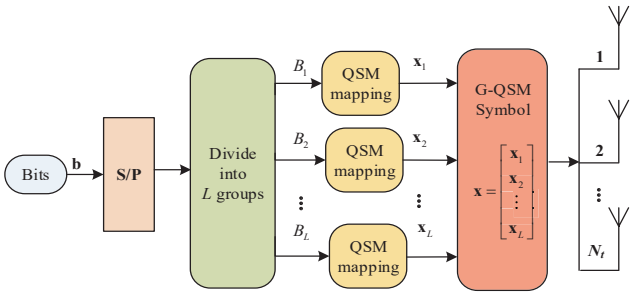

Fig. 1. System model of the proposed G-QSM system

of information bits having a length of $R_i = 2\log_2(N_Q^i) + \log_2(M_i)$ can be mapped to a QSM symbol as

$$\mathbf{x}_i = \begin{cases} [\underbrace{0,...,0}_{l_\Re^i-1}, x_\Re^i + jx_\Im^i, \underbrace{0,...,0}_{N_Q^i-l_\Re^i}]^T, \text{ if } l_\Re^i = l_\Im^i, \\ [\underbrace{0,...,0}_{l_\Re^i-1}, x_\Re^i, 0,...,0, jx_\Im^i, \underbrace{0,...,0}_{N_Q^i-l_\Im^i}]^T, \text{ else}, \end{cases} \tag{3}$$

where $x_\Re^i$ and $x_\Im^i$ denote the real and imaginary parts of x^i, respectively, while $l_\Re^i = (1,...,N_Q^i)$ and $l_\Im^i = (1,...,N_Q^i)$ represent the corresponding active TA indices. Hence, the transmitted signal of the G-QSM system can be expressed as

$$\mathbf{x} = [\mathbf{x}_1^T, \mathbf{x}_2^T, ..., \mathbf{x}_L^T]^T. \tag{4}$$

Let $\mathbf{H} \in \mathbb{C}^{N_r \times N_t}$ and $\mathbf{n} \in \mathbb{C}^{N_r \times 1}$ be the MIMO channel matrix and noise vector, whose entries are complex-valued Gaussian distributed, yielding $\mathcal{CN}(0,1)$ and $\mathcal{CN}(0,\sigma^2)$, respectively. The received signal $\mathbf{y} \in \mathbb{C}^{N_r \times 1}$ is written as

$$\mathbf{y} = \mathbf{H}\mathbf{x} + \mathbf{n}. \tag{5}$$

It follows from Eq. (4) that the optimal ML-based demodulator can be formulated as

$$\hat{\mathbf{x}}_{\text{ML}} = \arg\min_{\mathbf{x}\in\mathbb{X}} \|\mathbf{y} - \mathbf{H}\mathbf{x}\|^2, \tag{6}$$

where $\mathbb{X}$ is G-QSM symbol set associated with size of 2^R.

Achievable Rate of the G-QSM system

In this section, the bits/channel use (bpcu) throughput of the G-QSM system is analyzed. According to the system model of the G-QSM system, the transmit rate of the G-QSM system is formulated as

$$R = \sum_{i=1}^{L} [2\log_2(N_Q^i) + \log_2(M_i)]. \tag{7}$$

where N_Q^i is a power of 2[1]. The transmission rates of the SM-VBLAST and VBLAST are given as follows

$$\begin{aligned} R_{\text{SM-VBLAST}} &= \sum_{i=1}^{L} [\log_2(N_Q^i) + \log_2(M_i)], \\ R_{\text{VBLAST}} &= \sum_{i=1}^{L} \log_2(M_i). \end{aligned} \tag{8}$$

For a fixed value of L and $M_i = M$, the maximum transmission rate can be optimized as follows

$$\begin{aligned} R_{\max} &= \max_{N_Q^i} [\sum_{i=1}^{L} 2\log_2(N_Q^i) + \log_2(M)L] \\ s.t. &\sum_{i=1}^{L} N_Q^i = N_t, N_Q^i = 2^{(R_i - \log_2(M))/2}. \end{aligned} \tag{9}$$

Then the optimization problem can be analyzed for the following two cases

1) If N_t is a power of 2 with $N_t = 2^c$, the optimization problem is represented as

$$\begin{aligned} R_{\max} &= \max_{B_i} 2\sum_{i=1}^{L} B_i + L\log_2(M), \\ s.t. &\sum_{i=1}^{L} 2^{B_i} = 2^c, B_i = (1,2,...,c-1), \end{aligned} \tag{10}$$

where $B_i = \log_2(N_Q^i)$.

2) If N_t is not a power of 2 with $2^c < N_t < 2^{c+1}$, the optimization problem is represented as

$$\begin{aligned} R_{\max} &= \max_{B_i} 2\sum_{i=1}^{L} (B_i) + L\log_2(M), \\ s.t. &\sum_{i=1}^{L} 2^{B_i} = N_t, B_i = (1,2,...,c). \end{aligned} \tag{11}$$

To acquire the values $N_Q^1,...,N_Q^L$, $L-1$ decompositions are needed for N_t TAs. For the l-th $1 \le l \le L-1$ decomposition, we have $N_Q^1 = 2^{c_1}, N_Q^2 = 2^{c_2}, \cdots N_Q^2 = 2^{c_l}$ $c_1 \le c_2 \le \cdots \le c_l$ and the transmit rate becomes $R_l = \sum_{i=1}^{l} 2c_i + \log_2(M)l$. In the $(l+1)$-th decomposition, we choose any N_Q^i to be divided into the values of $N_Q^i/2, N_Q^i/2$, so the transmit rate becomes $R_{l+1} = 2(c_1 + \cdots + c_{i-1} + c_i - 1 + c_i - 1 + c_{i+1} + \cdots + c_l) + \log_2(M)l + \log_2(M)$. Accordingly, we have

$$R_{l+1} = R_l + 2(c_i - 2) + \log_2(M). \tag{12}$$

Hence, the different selection of c_i results in different transmission rates.

In [20], we introduce the so-called Large Number First (LNF) principle to obtain $N_Q^1,...,N_Q^L$. For the LNF principle, in the l-th $l \in (2,...,L\text{-}1)$ step, the largest number N_{l-1}^{lar} in the $(l-1)$-st set $\mathcal{N}_{l-1}$ is decomposed into two identical numbers as $(N_{l-1}^{lar}/2, N_{l-1}^{lar}/2)$, where $\mathcal{N}_1 = [N_t]$.

[1]For simplicity, in this paper, we have focused our attention on the achievable transmit rate of the proposed G-QSM system associated with N_Q^i being a power of 2. When N_Q^i is not a power of 2, the mapping scheme of [19] designed for an arbitrary number of antennas can be employed and the achievable transmit rate analysis following a similar process.

As a result, the decomposed set in the l-th step can be expressed as $\mathcal{N}_l = (\mathcal{N}_{l-1} \backslash N_{l-1}^{lar}, N_{l-1}^{lar}/2, N_{l-1}^{lar}/2)$. These processes continue, until we get L values as $N_Q^1, ..., N_Q^L$. Next, we will demonstrate by the mathematical techniques of induction that the LNF principle invoked for both cases of $N_t = 2^c$ and $N_t \neq 2^c$ can always achieve the maximum transmission rate of (9).

In the $k = 1$-st decomposition associated with N_t TAs, there are two cases, namely

1) If $N_t = 2^c$, we have $L = 2$ and $N_Q^1 = N_Q^2 = 2^{c-1}$, so that we have $B_1 = B_2 = c - 1$ in order to satisfy (10);
2) If $2^c < N_t < 2^{c+1}$ with $N_t = \sum_{i=1}^{m} 2^{c_i}$ [2], we have $L = m$ and $N_Q^1 = 2^{c_1}, N_Q^2 = 2^{c_2}, \cdots, N_Q^m = 2^{c_m}$, so that we have $B_1 = c_1, B_2 = c_2, ..., B_m = c_m$ in order to satisfy (11).

Hence, the maximum transmission rate $R_{k=1}$ of the $(k = 1)$-st decomposition is expressed as

$$R_{k=1} = \begin{cases} 2(2c-2) + 2\log_2(M), \text{if } N_t = 2^c, \\ \sum_{i=1}^{m} 2c_i + m\log_2(M), \text{else.} \end{cases} \quad (13)$$

1) If $k = 2$, we have $L = 3$ or $L = m + 1$. According to (12) and the LNF principle, we have
   a) If $N_t = 2^c$, we have $L = 3$ and $N_Q^1 = N_Q^2 = 2^{c-2}, N_Q^3 = 2^{c-1}$ with $B_1 = B_2 = c - 2, B_3 = c - 1$;
   b) If $2^c < N_t < 2^{c+1}$ with $N_t = \sum_{i=1}^{m} 2^{c_i}$, $c_1 \leq c_2 \leq \cdots \leq c_m$, we have $L = m + 1$ and $N_Q^1 = 2^{c_1}, N_Q^2 = 2^{c_2}, \cdots, N_Q^m = N_Q^{m+1} = 2^{c_m - 1}$ with $B_1 = c_1, B_2 = c_2, ..., B_m = B_{m+1} = c_m - 1$.

   Hence, according to (12)-(13), $R_{k=2}$ can be simplified to

$$R_{k=2}^{\text{LNF}} = \begin{cases} R_{k=1} + 2(c-1-2) + \log_2(M), \text{if } N_t = 2^c, \\ R_{k=1} + 2(c_m - 2) + \log_2(M), \text{else.} \end{cases} \quad (14)$$

   It is evident that the LNF principle is capable of achieving the maximum transmission rate $R_{\max}$.
2) Assuming that the $(k = K)$-th decomposition associated with $c_1, c_2, ..., c_K$ has the maximum transmit rate $R_{\max}^K$, according to (12), the maximum rate of the $(K + 1)$-st decomposition is expressed as

$$R_{\max}^{K+1} = R_{\max}^K + \max_i 2(c_i - 2) + \log_2(M). \quad (15)$$

   It is evident that the LNF principle allows (15) to achieve the maximum transmission rate of (9).
3) Based on the analysis of 1) and 2), it is concluded that the LNF principle allows (9) to remain true for any value of N_t in conjunction with L $(1 \leq L \leq N_t/2)$.

In order to provide further insights, Figs.2-3 present the achievable rate of the QPSK aided SM-VBLAST and of the proposed G-QSM system for different values of L and N_t. Observe from Fig. 2 that the rate achieved by the G-QSM system is significantly higher than that of the SM-VBLAST system for a fixed value of L. The higher the value of L is, the higher the rate advantage becomes. More specifically, for a small value of $L = 8$, the transmission rate of the proposed G-QSM system may reach 128 bpcu, while that of the SM-VBLAST system is 72 bpcu. Observe from Fig. 3 that the rate achieved by the G-QSM system is significantly increased as L increases. The transmission rate of the G-QSM system for $N_t = 1024, L = 64$ becomes 640 bpcu, while that of the SM-VBLAST system is 384 bpcu. Hence, the proposed G-QSM system achieves a high throughput, despite using a low number of RF chains.

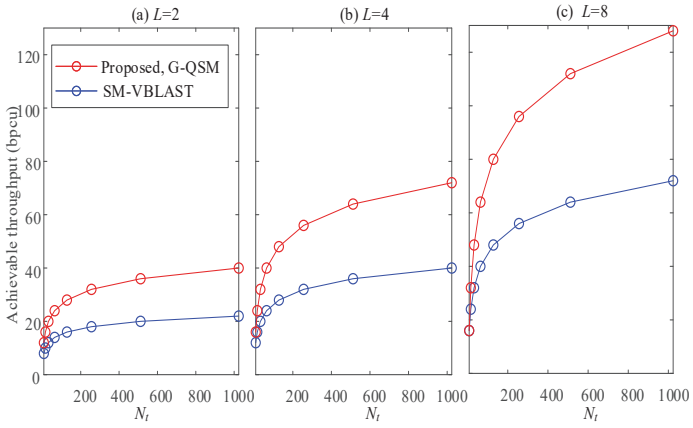

Fig. 2. The achievable rate of the QPSK aided SM-VBLAST and of the proposed G-QSM system having diverse values of N_t and a fixed value of L. a) $L = 2$; b) $L = 4$; c) $L = 8$.

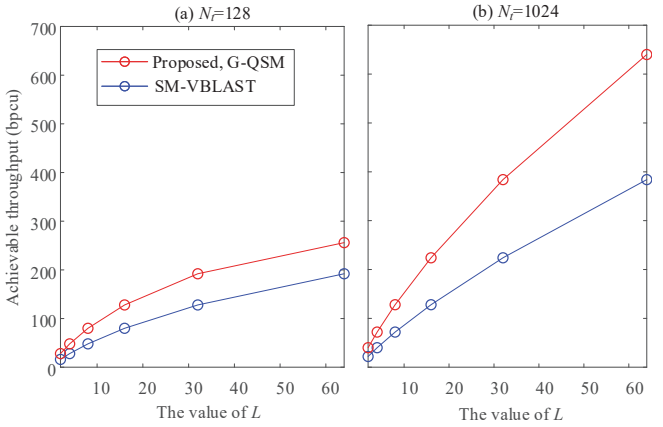

Fig. 3. The achievable rate of the QPSK aided SM-VBLAST and of the proposed G-QSM system having a fixed number of TAs and different values of L. a) $N_t = 128$; b) $N_t = 1024$.

Bit-to-Symbol Mapping and Symbol-to-Bit Demapping

In this section, the bit-to-symbol mapping and symbol-to-bit demapping are introduced for our G-QSM system.

Symbol-to-Bit Mapping

The symbol-to-bit mapping of the proposed G-QSM system is introduced in detail as follows.

[2]In this case, $L = m$ is the smallest number that the decomposition can have. Taking $N_t = 12$ and $N_t = 14$ for example, we have $L = 2$ and $L = 3$, respectively.

Step 1: Obtain the numbers $(N_Q^1, N_Q^2, ..., N_Q^L)$ for constructing the QSM symbols based on the LNF principle [26].

Step 2: Construct the i-th QSM symbol $\mathbf{x}_i$ using N_Q^i TAs and obtain the indices $(q_{\Re}^i, q_{\Im}^i)$ of the real and imaginary parts of x_i.

Step 3: Obtain the whole G-QSM symbol $\mathbf{x}$ by (4) based on the L obtained QSM symbols of Step 2. Assuming that $(l_{\Re}^i, l_{\Im}^i)$ are the indices of the real and imaginary parts of x_i in the $\mathbf{x}$, the relationship between $(l_{\Re}^i, l_{\Im}^i)$ and $(q_{\Re}^i, q_{\Im}^i)$ is expressed as

$$l_{\Re}^i = \sum_{t=1}^{i-1} N_Q^t + q_{\Re}^i; l_{\Im}^i = \sum_{t=1}^{i-1} N_Q^t + q_{\Im}^i. \tag{16}$$

Symbol-to-Bit Demapping

At the receiver, the symbol-to-bit de-mapping processes rely on the values of $(N_Q^1, ..., N_Q^L)$ and the values of $(l_{\Re}^i, l_{\Im}^i, x_i)$ $(i = 1, ..., L)$, which operate in detail as follows.

Step 1: Obtain the values of $(q_{\Re}^i, q_{\Im}^i, x_i)$ $(i = 1, ..., L)$ based on the detector and (15).

Step 2: Demodulate $(q_{\Re}^i, q_{\Im}^i)$ into the information bits according to $\mathbf{b}_{\Re}^i = \text{de2bi}[q_{\Re}^i, \log_2(N_Q^i)]$ and $\mathbf{b}_{\Im}^i = \text{de2bi}[q_{\Im}^i, \log_2(N_Q^i)]$, where $\text{de2bi}(m, n)$ is a function that transforms a decimal number m to n bits. Demodulation x_i into information bits generates $\mathbf{b}_x^i$. Hence the i-th QSM symbol is demodulated into bits as $\mathbf{b}_i = [\mathbf{b}_{\Re}^i, \mathbf{b}_{\Im}^i, \mathbf{b}_x^i]$.

Step 3: Finally, we obtain the demodulated bits as $\mathbf{b} = [\mathbf{b}_1, ..., \mathbf{b}_i, ..., \mathbf{b}_L]$.

Performance Analysis for the Proposed Generalized QSM System

The ABEP of the Proposed G-QSM System

Let us denote the transmit signal and receive signal of our G-QSM system by $\mathbf{x}^i = [\mathbf{x}_1^i, ..., \mathbf{x}_L^i]$ and $\mathbf{x}^j = [\mathbf{x}_1^j, ..., \mathbf{x}_L^j]$, respectively. The ABEP upper bound is given by

$$P_b = \frac{1}{R2^R} \sum_{i=1}^{2^R} \sum_{j=1, j\neq i}^{2^R} d(\mathbf{x}^i, \mathbf{x}^j) P(\mathbf{x}^i \to \mathbf{x}^j), \tag{17}$$

where $P(\mathbf{x}^i \to \mathbf{x}^j)$ denotes the Pairwise Error Probability (PEP), $d(\mathbf{x}^i, \mathbf{x}^j)$ is the Hamming Distance (HD) associated with the corresponding PEP event. According to [20], $P(\mathbf{x}^i \to \mathbf{x}^j)$ is expressed as

$$P(\mathbf{x}^i \to \mathbf{x}^j) = F(\bar{\zeta}) = \gamma(\bar{\zeta})^{N_r} \sum_{k=0}^{N_r-1} \binom{N_r - 1 + k}{k} [1 - \gamma(\bar{\zeta})]^k, \tag{18}$$

where $\gamma(\bar{\zeta}) = \frac{1}{2}\left(1 - \sqrt{\frac{\bar{\zeta}/2}{1+\bar{\zeta}/2}}\right)$ and $\bar{\zeta}$ is the mean value of $\zeta = \|\mathbf{H}(\mathbf{x}^i - \mathbf{x}^j)\|^2/2\sigma^2$ with $N_r = 1$ as

$$\bar{\zeta} = E\{\|\mathbf{H}(\mathbf{x}^i - \mathbf{x}^j)\|^2/2\sigma^2 | N_r = 1\} = \|(\mathbf{x}^i - \mathbf{x}^j)\|^2/2\sigma^2. \tag{19}$$

According to (17), the ABEP is obtained by calculating 2^{2R} PEP events and HDs, which becomes impractical in scenarios having a high throughput. In order to evaluate the large-scale G-QSM's performance, simplified ABEP upper bound expressions are derived. Specifically, for QPSK modulation, Eq. (17) can be further simplified to

$$P_b = \frac{1}{R} \sum_{j=2}^{2^R} d(\mathbf{x}^1, \mathbf{x}^j) P(\mathbf{x}^1 \to \mathbf{x}^j). \tag{20}$$

For 16-QAM modulation, (17) cannot be represented by (20), hence the simplified ABEP upper bound calculation becomes again more complicated. Hence, the simplified ABEP upper bound expressions analysis are only valid for our proposed G-QSM system using QPSK modulation, whilst other high-order schemes will be consider in our future work. Specifically, according to [20], there are only n different values $\bar{\zeta}$ as $\bar{\zeta}_1$,...,$\bar{\zeta}_n$ in (18), Eq. (20) can be finally simplified to

$$\begin{aligned} P_b &= \frac{\sum_{t=1}^{\varphi_1} d_{\bar{\zeta}_1}^t F(\bar{\zeta}_1) + \sum_{t=1}^{\varphi_2} d_{\bar{\zeta}_2}^t F(\bar{\zeta}_2) + \cdots + \sum_{t=1}^{\varphi_n} d_{\bar{\zeta}_2}^t F(\bar{\zeta}_n)}{R}, \\ &= D(\bar{\zeta}_1)F(\bar{\zeta}_1) + D(\bar{\zeta}_2)F(\bar{\zeta}_2) + \cdots + D(\bar{\zeta}_n)F(\bar{\zeta}_n) \end{aligned} \tag{21}$$

with

$$\begin{aligned} &D(\bar{\zeta}_p) = \frac{\sum_{t=1}^{\varphi_p} d_{\bar{\zeta}_p}^t}{R}, p = 1, ..., n, \\ &\sum_{t=1}^{\varphi_1} d_{\bar{\zeta}_1}^t + \cdots + \sum_{t=1}^{\varphi_n} d_{\bar{\zeta}_n}^t = \sum_{j=1}^{2^R} d\left(\mathbf{x}^1, x^j\right) = \sum_{r=1}^{R} C_R^r r = R2^{R-1}, \end{aligned} \tag{22}$$

where φ_p is the number of $\bar{\zeta}_p$ for $(\mathbf{x}^1, \mathbf{x}^j)$ and $\sum_{r=1}^{R} C_R^r r = R2^{R-1}$, which can be seen in the Appendix. As a result, the calculation of ABEP only has to find the n different values of $\bar{\zeta}_1$,...,$\bar{\zeta}_n$ and to compute their corresponding values of $F(\bar{\zeta}_1)$,...,$F(\bar{\zeta}_n)$ and $D(\bar{\zeta}_1), ..., D(\bar{\zeta}_n)$. Furthermore, $F(\bar{\zeta}_1)$,...,$F(\bar{\zeta}_n)$ can be obtained by (17), so that the calculation of $D(\bar{\zeta}_1), ..., D(\bar{\zeta}_n)$ is the key issue, which is introduced in detail as follows.

ABEP of G-QSM with $L = 1$

The system model of the G-QSM system with $L = 1$ is the same as that of the QSM system. In this section, a simplified expression of ABEP upper bound is derived for large-scale QSM system. Assuming that $l_{\Re}^i$, $l_{\Im}^i$, $x_{\Re}^i$, $x_{\Im}^i$ are the antenna indices and symbols of the QSM symbol $\mathbf{x}^i$, the Euclidean Distance (ED) between $\mathbf{x}^i$ and x^j is given by:

$$\begin{aligned} &\left\|\mathbf{x}^i - \mathbf{x}^j\right\|^2 \\ &= \begin{cases} |x_{\Re}^i - x_{\Re}^j|^2 + |x_{\Im}^i - x_{\Im}^j|^2, & \text{if } l_{\Re}^i = l_{\Re}^j, l_{\Im}^i = l_{\Im}^j; \\ |x_{\Re}^i - x_{\Re}^j|^2 + |x_{\Im}^i|^2 + |x_{\Im}^j|^2, & \text{if } l_{\Re}^i = l_{\Re}^j, l_{\Im}^i \neq l_{\Im}^j; \\ |x_{\Re}^i|^2 + |x_{\Re}^j|^2 + |x_{\Im}^i - x_{\Im}^j|^2, & \text{if } l_{\Re}^i \neq l_{\Re}^j, l_{\Im}^i = l_{\Im}^j; \\ |x_{\Re}^i|^2 + |x_{\Im}^i|^2 + |x_{\Re}^j|^2 + |x_{\Im}^j|^2, & \text{if } l_{\Re}^i \neq l_{\Re}^j, \Im^i \neq l_{\Im}^j. \end{cases} \end{aligned} \tag{23}$$

For the case of QPSK modulation, there are only 4 different values of $\bar{\zeta}_1 = 1/2\sigma^2$, $\bar{\zeta}_2 = 2/2\sigma^2$, $\bar{\zeta}_3 = 3/2\sigma^2$ and $\bar{\zeta}_4 = 4/2\sigma^2$ for each different i in 2^R EDs $\left\|\mathbf{x}^i - \mathbf{x}^j\right\|^2$ $j = (1, ..., 2^R)$, so that (17) can be represented to (20). For the case of 16-QAM,

2^R EDs $\left\|\mathbf{x}^i-\mathbf{x}^j\right\|^2$ $j=(1,...,2^R)$ are different for different values of i. Specifically, we have $||\mathbf{x}_i-\mathbf{x}_j||^2 \in \{0.2,0.4,0.6,0.8,1,1.2,1.4,1.6,1.8,2,2.2,2.6,2.8,3.2,3.4,3.6,3.8,4,4.6,5.2,5.4,7.2\}$ for 16-QAM. For the transmit signal $\mathbf{x}_1$, we have $||\mathbf{x}_1-\mathbf{x}_j||^2 \in \{0.4,0.8,1,1.4,1.6,1.8,2,2.2,2.6,2.8,3.2,3.4,3.6,4,4.6,5.2,5.4,7.2\}$, while $||\mathbf{x}_2-\mathbf{x}_j||^2 \in \{0.2,0.4,0.6,0.8,1,1.2,1.41.6,1.8,2,2.2,2.6,2.8,3.2,3.4,3.6,3.8,4,4.6,5.2\}$ for $(j=1,...,2^R)$ holds for $\mathbf{x}_2$, hence (17) cannot be represented by (20). For the large-scale QPSK aided QSM ABEP calculation, we only have to compute four corresponding values of $F(\bar{\varsigma}_1)$,...,$F(\bar{\varsigma}_4)$ and $D(\bar{\varsigma}_1),...,D(\bar{\varsigma}_4)$.

Specifically, the information bits of the G-QSM system with $L=1$ conveyed consists of four parts: $\mathbf{b}_\Re$, $\mathbf{b}_\Im$, $c_\Re$ and $c_\Im$, where $\mathbf{b}_\Re$ is the bit vector that is conveyed by the real symbol index, $\mathbf{b}_\Im$ is the bit vector conveyed by the imaginary symbol index, $c_\Re$ is the bit vector conveyed by the real symbol, and $c_\Im$ is the bit vector conveyed by the imaginary symbol. Due to the symmetry, we set $i=1$ for simplicity. The information bit vectors that the $\mathbf{x}^1$ and $\mathbf{x}^j$ symbols conveyed can be expressed as

$$\begin{aligned}\mathbf{x}^1 &\rightarrow [\underbrace{0,...,0}_{\mathbf{b}^1_\Re},\underbrace{0,...,0}_{\mathbf{b}^1_\Im},\underbrace{0}_{c^1_\Im},\underbrace{0}_{c^1_\Re}],\\ \mathbf{x}^j &\rightarrow [\underbrace{b_{r,1},...,b_{r,B}}_{\mathbf{b}^j_\Re},\underbrace{b_{j,1},...,b_{j,B}}_{\mathbf{b}^j_\Im},\underbrace{c_1}_{c^j_\Im},\underbrace{c_2}_{c^j_\Re}].\end{aligned} \tag{24}$$

Then the HDs between $(\mathbf{b}^1_\Re,\mathbf{b}^j_\Re)$, $(\mathbf{b}^1_\Im,\mathbf{b}^j_\Im)$, $(\mathbf{c}^1_\Re,\mathbf{c}^j_\Re)$ and $(\mathbf{c}^1_\Im,\mathbf{c}^j_\Im)$ are defined as

$$\begin{aligned}d^r_{\bar{\zeta}} &= \mathrm{Diff}(\mathbf{b}^1_\Re,\mathbf{b}^j_\Re)\in\mathbb{B}=[0,\underbrace{1,...,1}_{C^1_B},...,\underbrace{b,...,b}_{C^b_B},...,\underbrace{B}_{C^B_B}],\\ d^j_{\bar{\zeta}} &= \mathrm{Diff}(\mathbf{b}^1_\Im,\mathbf{b}^j_\Im)\in\mathbb{B}=[0,\underbrace{1,...,1}_{C^1_B},...,\underbrace{b,...,b}_{C^b_B},...,\underbrace{B}_{C^B_B}],\\ d^i_{\bar{\zeta}} &= \mathrm{Diff}([c^1_\Im,c^j_\Im]\in\mathbb{P}, d^q_{\bar{\zeta}}=\mathrm{Diff}([c^1_\Re,c^j_\Re]\in\mathbb{P},\end{aligned} \tag{25}$$

where $B=\log_2(N_t), b\in(0,B)$, $\mathrm{Diff}(x,y)$ is a function returning the difference between x and y, $\mathbb{B}$ is the HD set of the bits that antenna indices conveyed, and $\mathbb{P}$ is the HD set of the bits that the AMP symbols carried and we have $\mathbb{P}=[0,1]$ for QPSK. Then the Average HD (AHD) between $\mathbf{x}^1$ and $\mathbf{x}^j$ can be represented as

$$D(\bar{\zeta})=\frac{\sum d_{\bar{\zeta}}}{R}=\frac{\sum_{i=1}^{2}\sum_{q=1}^{2}\sum_{j=1}^{2^B}\sum_{r=1}^{2^B}(d^i_{\bar{\zeta}}+d^q_{\bar{\zeta}}+d^j_{\bar{\zeta}}+d^r_{\bar{\zeta}})}{2B+2}. \tag{26}$$

According to (23)-(24), the values of $D(\bar{\varsigma}_1),...,D(\bar{\varsigma}_4)$ are counted as follows.

Case 1 $\bar{\zeta}_1=1/2\sigma^2$**:** According to (21), there are two scenarios $l^1_\Re\neq l^j_\Re, l^1_\Im=l^j_\Im, x^1_\Im=x^j_\Im$ and $l^1_\Im\neq l^j_\Im, l^1_\Re=l^j_\Re, x^1_\Re=x^j_\Re$ having the result of $\bar{\zeta}_1=1/2\sigma^2$. The HDs between $\mathbf{x}^1$ and $\mathbf{x}^j$ for these two cases are computed as follows.

1) If $l^1_\Re\neq l^2_\Re, l^1_\Im=l^2_\Im, x^1_\Im=x^2_\Im$ is satisfied, we have the following HDs as $d^j_{\bar{\zeta}}=d^q_{\bar{\zeta}}=0$, $d^r_{\bar{\zeta}}\neq 0$, and $d^i_{\bar{\zeta}}\in[0,1]$. There are a total of $\varphi_{1,1}=2\times(2^B-1)$ scenarios having this result, so that the total HDs between $\mathbf{x}^1$ and $\mathbf{x}^j$ in these conditions can be expressed as

$$\begin{aligned}H_{1,1}&=\sum_{i=1}^{2}\sum_{r=2}^{2^B}(d^i_{\bar{\zeta}}+d^r_{\bar{\zeta}})=(2^B-1)\sum_{i=1}^{2}d^i_{\bar{\zeta}}+2\times\sum_{r=2}^{2^B}d^r_{\bar{\zeta}}\\&=(2^B-1)+2\sum_{b=1}^{B}C^b_B b.\end{aligned} \tag{27}$$

2) If $l^1_\Im\neq l^2_\Im, l^1_\Re=l^2_\Re, x^1_\Re=x^2_\Re$ is satisfied, we have $d^r_{\bar{\zeta}}=d^i_{\bar{\zeta}}=0$, $d^j_{\bar{\zeta}}\neq 0$ and $d^q_{\bar{\zeta}}\in[0,1]$. There are also a total of $\varphi_{1,2}=2\times(2^B-1)$ scenarios having this result, so that the total HDs between $\mathbf{x}^1$ and $\mathbf{x}^j$ in these conditions can be expressed as

$$\begin{aligned}H_{1,2}&=\sum_{q=1}^{2}\sum_{j=2}^{2^B}(d^q_{\bar{\zeta}}+d^j_{\bar{\zeta}})\\&=(2^B-1)\sum_{q=1}^{2}d^q_{\bar{\zeta}}+2\times\sum_{j=2}^{2^B}d^j_{\bar{\zeta}}=(2^B-1)+2\sum_{b=1}^{B}C^b_B b.\end{aligned} \tag{28}$$

Hence, the AHD $D(\bar{\varsigma}_1)$ is computed by

$$D(\bar{\varsigma}_1=\frac{1}{2\sigma^2})=\frac{H_1}{R}=\frac{H_{1,1}+H_{1,2}}{2B+2}=\frac{2(2^B-1)+4\sum_{b=1}^{B}C^b_B b}{2B+2}, \tag{29}$$

and the total number of conditions having $\bar{\zeta}_1=1/2\sigma^2$ is expressed as $\varphi_1=\varphi_{1,1}+\varphi_{1,2}=4(2^B-1)$.

Case 2 $\bar{\zeta}_2=2/2\sigma^2$**:** According to (21), there are three conditions $(l^1_\Re\neq l^2_\Re, l^1_\Im\neq l^2_\Im)$, $(l^1_\Im=l^2_\Im, l^1_\Re=l^2_\Re, x^1_\Re=x^2_\Re, x^1_\Im\neq x^2_\Im)$, $(l^1_\Im=l^2_\Im, l^1_\Re=l^2_\Re, x^1_\Im=x^2_\Im, x^1_\Re\neq x^2_\Re)$ having the result of $\bar{\zeta}_2=2/2\sigma^2$. The total HDs for these three cases are computed as follows.

1) If $l^1_\Re\neq l^2_\Re, l^1_\Im\neq l^2_\Im$ is satisfied, we have $d^j_{\bar{\zeta}}\neq 0$, $d^r_{\bar{\zeta}}\neq 0$, $d^i_{\bar{\zeta}}\in[0,1]$, $d^q_{\bar{\zeta}}\in[0,1]$. There are a total of $\varphi_{2,1}=4(2^B-1)^2$ scenarios having this result, so that the total HDs between $\mathbf{x}^1$ and $\mathbf{x}^j$ in these conditions can be expressed as

$$\begin{aligned}H_{2,1}&=\sum_{i=1}^{2}\sum_{q=1}^{2}\sum_{j=2}^{2^B}\sum_{r=2}^{2^B}(d^i_{\bar{\zeta}}+d^q_{\bar{\zeta}}+d^j_{\bar{\zeta}}+d^r_{\bar{\zeta}})\\&=2w^2\sum_{i=1}^{2}d^i_{\bar{\zeta}}+2w^2\sum_{i=1}^{2}d^q_{\bar{\zeta}}+4w\sum_{i=1}^{2}d^j_{\bar{\zeta}}+4w\sum_{i=1}^{2}d^r_{\bar{\zeta}}\\&=2w^2+2w^2+8w\sum_{b=1}^{B}C^b_B b,\end{aligned} \tag{30}$$

where $w=2^B-1$.

2) If $l^1_\Im=l^2_\Im, l^1_\Re=l^2_\Re, x^1_\Re=x^2_\Re, x^1_\Im\neq x^2_\Im$ is satisfied, we have $d^i_{\bar{\zeta}}=d^j_{\bar{\zeta}}=d^r_{\bar{\zeta}}=0, d^q_{\bar{\zeta}}=1$. There is only one $\varphi_{2,2}=1$ scenario having this result, hence the HD for this case can be expressed as

$$H_{2,2}=d^i_{\bar{\zeta}}+d^j_{\bar{\zeta}}+d^r_{\bar{\zeta}}+d^q_{\bar{\zeta}}=1. \tag{31}$$

3) If $l^1_\Im=l^2_\Im, l^1_\Re=l^2_\Re, x^1_\Im=x^2_\Im, x^1_\Re\neq x^2_\Re$ is satisfied, we have $d^q_{\bar{\zeta}}=d^j_{\bar{\zeta}}=d^r_{\bar{\zeta}}=0, d^i_{\bar{\zeta}}=1$. There is only one $\varphi_{2,3}=1$ scenario having this result, hence the HD

for this case can be formulated as

$$H_{2,3} = d^i_{\bar{\zeta}} + d^j_{\bar{\zeta}} + d^r_{\bar{\zeta}} + d^q_{\bar{\zeta}} = 1. \tag{32}$$

Hence, the AHD $D(\bar{\varsigma}_2)$ between $\mathbf{x}^1$ and $\mathbf{x}^j$ having $\bar{\zeta}_2 = 2/2\sigma^2$ is expressed by

$$D(\bar{\varsigma}_2 = \tfrac{2}{2\sigma^2}) = \tfrac{H_2}{R} = \tfrac{H_{2,1}+H_{2,2}+H_{2,3}}{2B+2} = \tfrac{4w^2+8w\sum_{b=1}^{B} C_B^b b+2}{2B+2}, \tag{33}$$

and the total number of conditions having $\bar{\zeta}_2 = 2/2\sigma^2$ is expressed as $\varphi_2 = 4(2^B-1)^2+2$.

Case 3 $\bar{\zeta}_1 = 3/2\sigma^2$**:** According to (21), there are two conditions as $l^1_{\Re} \neq l^2_{\Re}, l^1_{\Im} = l^2_{\Im}, x^1_{\Im} \neq x^2_{\Im}$ and $l^1_{\Re} = l^2_{\Re}, l^1_{\Im} \neq l^2_{\Im}, x^1_{\Re} \neq x^2_{\Re}$ having the result of $\bar{\zeta}_3 = 3/2\sigma^2$. The HDs for these two cases are computed as follows.

1) If $l^1_{\Re} \neq l^2_{\Re}, l^1_{\Im} = l^2_{\Im}, x^1_{\Im} \neq x^2_{\Im}$ is satisfied, we have $d^r_{\bar{\zeta}} \neq 0, d^j_{\bar{\zeta}} = 0, d^q_{\bar{\zeta}} = 1, d^i_{\bar{\zeta}} = [0,1]$. There are a total of $\varphi_{3,1} = 2(2^B-1)$ scenarios having this result, so that the HDs for these cases can be expressed as

$$H_{3,1} = \sum_{i=1}^{2}\sum_{r=2}^{2^B}(d^i_{\bar{\zeta}} + 1 + d^r_{\bar{\zeta}}) = 3(2^B-1) + 2\sum_{b=1}^{B} C_B^b b. \tag{34}$$

2) If $l^1_{\Re} = l^2_{\Re}, l^1_{\Im} \neq l^2_{\Im}, x^1_{\Re} \neq x^2_{\Re}$ is satisfied, we have $d^r_{\bar{\zeta}} = 0, d^j_{\bar{\zeta}} \neq 0, d^i_{\bar{\zeta}} = 1$ and $d^i_{\bar{\zeta}} \in [0,1]$. There are a total of $\varphi_{3,2} = 2(2^B-1)$ scenarios having this result, so that the HDs for these cases can be expressed as

$$H_{3,2} = \sum_{q=1}^{2}\sum_{j=2}^{2^B}(d^q_{\bar{\zeta}} + 1 + d^j_{\bar{\zeta}}) = 3(2^B-1) + 2\sum_{b=1}^{B} C_B^b b. \tag{35}$$

As a result, the AHD $D(\bar{\varsigma}_3)$ between $\mathbf{x}^1$ and $\mathbf{x}^j$ having $\bar{\zeta}_3 = 3/2\sigma^2$ is formulated as

$$D(\bar{\varsigma}_3 = \tfrac{3}{2\sigma^2}) = \tfrac{H_3}{R} = \tfrac{H_{3,1}+H_{3,2}}{2B+2} = \tfrac{2[3(2^B-1)+2\sum_{b=1}^{B} C_B^b b]}{2B+2}, \tag{36}$$

and the total number of conditions having $\bar{\zeta}_3 = 3/2\sigma^2$ is expressed as $\varphi_3 = \varphi_{3,1} + \varphi_{3,2} = 4(2^B-1)$.

Case 4 $\bar{\zeta}_4 = 4/2\sigma^2$**:** According to (21), there is only one condition $l^1_{\Re} = l^2_{\Re}, l^1_{\Im} = l^2_{\Im}, x^1_{\Re} \neq x^2_{\Re}, x^1_{\Im} \neq x^2_{\Im}$ having the result of $\bar{\zeta}_4 = 4/2\sigma^2$. In this case, we have $d^r_{\bar{\zeta}} = 0, d^j_{\bar{\zeta}} = 0, d^i_{\bar{\zeta}} = d^q_{\bar{\zeta}} = 1$, the AHD between $\mathbf{x}^1$ and $\mathbf{x}^j$ is expressed as

$$D(\bar{\varsigma}_4 = \frac{4}{2\sigma^2}) = \frac{H_4}{R} = \frac{2}{2B+2}. \tag{37}$$

Since $\sum_{m=1}^{4}\varphi_m = 2^R - 1$, $\sum_{b=1}^{B} C_B^b b = B2^{B-1}$ and $H_1 + H_2 + H_3 + H_4 = \sum_{u=1}^{R} C_R^u u$, the ABEP of the G-QSM for $L=1$ can be obtained by

$$\begin{aligned} P_b^{L=1} = &\left[\frac{(B+1)2^B-1}{B+1}\right] F\left(\frac{1}{2\sigma^2}\right) + \\ &\left[\frac{(B+1)2^{2B+1}-(2B+4)2^B+3}{B+1}\right] F\left(\frac{1}{\sigma^2}\right) + \\ &\left[\frac{(B+3)2^B-3}{B+1}\right] F\left(\frac{3}{2\sigma^2}\right) + \left[\frac{1}{B+1}\right] F\left(\frac{2}{\sigma^2}\right). \end{aligned} \tag{38}$$

It is shown in (38) that the ABEP upper bound is obtained by only calculating as few as 4 PEP and HD events, while that in [21] has to calculate 2^{4B+4} PEP events and HDs, which becomes impractical for large-scale QSM systems. As a result, the expression derived in (38) becomes helpful for large-scale QSM systems performance evaluation.

ABEP of G-QSM with $L = 2$

For the case of $L=2$, we have $R = \sum_{l=1}^{2} 2B_l + 4$ with $B_l = \log_2(N_Q^l)$. Assuming that $\mathbf{x}^i$ and $\mathbf{x}^j$ are two different G-QSM symbols expressed as

$$\mathbf{x}^i = \begin{bmatrix} \mathbf{x}^i_1 \\ \mathbf{x}^i_2 \end{bmatrix}, \mathbf{x}^j = \begin{bmatrix} \mathbf{x}^j_1 \\ \mathbf{x}^j_2 \end{bmatrix}, \tag{39}$$

the ED between them can be computed as

$$\|\mathbf{x}^i - \mathbf{x}^j\|^2 = \left\| \begin{matrix} \mathbf{x}^i_1 - \mathbf{x}^j_1 \\ \mathbf{x}^i_2 - \mathbf{x}^j_2 \end{matrix} \right\|^2 = \|\mathbf{x}^i_1 - \mathbf{x}^j_1\|^2 + \|\mathbf{x}^i_2 - \mathbf{x}^j_2\|^2. \tag{40}$$

Assuming that $\mathbf{x}^i_1$ and $\mathbf{x}^i_2$ are mapped by the information bits $\mathbf{b}^i_1$ with length of $2B_1+2$ and $\mathbf{b}^i_2$ with length of $2B_2+2$, respectively, according to (21), there are five values $\{0,1,2,3,4\}$ for $\chi_1 = \|\mathbf{x}^i_1 - \mathbf{x}^j_1\|^2$ and $\chi_2 = \|\mathbf{x}^i_2 - \mathbf{x}^j_2\|^2$. Let us define $d^l_{\zeta_{n_l}} = \mathrm{Diff}(\mathbf{b}^i_l, \mathbf{b}^j_l)$ by the HD associated with $\chi_l = n_l$, $\varphi^l_{n_l}$ by the number of this case. The total HD associated with $\chi_l = n_l$, $l = 1,2$, $n_l = 0,1,2,3,4$ is given by $H^l_{n_l} = \sum d^l_{\zeta_{n_l}}$. According to (29), (33), (36) and (37), we have the following formulations

$$\{\chi_l\}_{l=1}^{L} = \begin{cases} 0 \rightarrow H^l_0 = 0, \\ 1 \rightarrow H^l_1 = 2^{B_l+1}(B_l+1) - 2, \\ 2 \rightarrow H^l_2 = [2^{2B_l+2}(B_l+1) - 2^{B_l+2}(2+B_l) + 6], \\ 3 \rightarrow H^l_3 = [2^{B_l+1}(3+B_l) - 6], \\ 4 \rightarrow H^l_4 = 2, \end{cases} \tag{41}$$

and

$$\begin{aligned} &\varphi^l_0 = 1, \varphi^l_1 = 4(2^{B_l}-1), \varphi^l_2 = 4(2^{B_l}-1)^2 + 2, \\ &\varphi^l_3 = 4(2^{B_l}-1), \varphi^l_4 = 1, \sum_{n=1}^{4}\varphi^l_n = 2^{2B_l+2}. \end{aligned} \tag{42}$$

According to (23) and (40), there are a total of 8 values of $\left\|\mathbf{x}^i - \mathbf{x}^j\right\|^2/(2\sigma^2) = (n_1+n_2)/(2\sigma^2)$ as

$$\begin{aligned} &\bar{\varsigma}_1 = \tfrac{1}{2\sigma^2} \leftrightarrow n_1{=}1, n_2{=}0; n_1{=}0, n_2 = 1; \\ &\bar{\varsigma}_2 = \tfrac{2}{2\sigma^2} \leftrightarrow n_1{=}2, n_2 = 0; n_1{=}0, n_2{=}2; n_1{=}n_2{=}1; \\ &\bar{\varsigma}_3 = \tfrac{3}{2\sigma^2} \leftrightarrow n_1{=}3, n_2 = 0; n_1{=}0, n_2{=}3; \\ &\qquad\qquad n_1{=}1, n_2{=}2; n_1{=}2, n_2{=}1; \\ &\bar{\varsigma}_4 = \tfrac{4}{2\sigma^2} \leftrightarrow n_1{=}4, n_2 = 0; n_1{=}0, n_2{=}4; n_1{=}n_2{=}2; \\ &\qquad\qquad n_1{=}1, n_2{=}3; n_1{=}3, n_2{=}1; \\ &\bar{\varsigma}_5 = \tfrac{5}{2\sigma^2} \leftrightarrow n_1{=}4, n_2 = 1; n_1{=}1, n_2{=}4; \\ &\qquad\qquad n_1{=}2, n_2{=}3; n_1{=}3, n_2{=}2; \\ &\bar{\varsigma}_6 = \tfrac{6}{2\sigma^2} \leftrightarrow n_1{=}4, n_2 = 2; n_1{=}2, n_2{=}4; n_1{=}n_2{=}3; \\ &\bar{\varsigma}_7 = \tfrac{7}{2\sigma^2} \leftrightarrow n_1{=}4, n_2 = 3; n_1{=}3, n_2{=}4; \\ &\bar{\varsigma}_8 = \tfrac{8}{2\sigma^2} \leftrightarrow n_1{=}4, n_2 = 4. \end{aligned} \tag{43}$$

The total HD between $\mathbf{x}^i$ and $\mathbf{x}^j$ associated with $\bar{\varsigma}_m = m/(2\sigma^2)$ $m = (1, ..., 8)$ is expressed as

$$H_m = \sum_{(n_1,n_2)} (H^1_{n_1} + H^2_{n_2}) = \sum\sum d^1_{\varsigma n_1} + d^2_{\varsigma n_2}, n_1 + n_2 = m. \tag{44}$$

According to (41)-(44), the values of H_m $m = (1, ..., 8)$ are calculated as

$$\begin{aligned} H_1 &= (\sum\sum d^1_{\zeta_0} + d^2_{\zeta_1}) + (\sum\sum d^1_{\zeta_1} + d^2_{\zeta_0}) \\ &= H^2_1 + H^1_1 = \sum_{l=1}^{2} [2^{B_l+1}(B_l + 1)] - 4, \end{aligned} \tag{45}$$

$$\begin{aligned} H_2 &= (\sum\sum d^1_{\zeta_0} + d^2_{\zeta_2}) + (\sum\sum d^1_{\zeta_2} + d^2_{\zeta_0}) + (\sum\sum d^1_{\zeta_1} + d^2_{\zeta_1}) \\ &= H^2_2 + H^1_2 + \sum_{s=1}^{\varphi^1_1} \sum_{t=1}^{\varphi^2_1} d^{1,s}_{\zeta_1} + d^{2,t}_{\zeta_1} \\ &= H^2_2 + H^1_2 + \varphi^1_1 H^2_1 + \varphi^2_1 H^1_1, \end{aligned} \tag{46}$$

$$\begin{aligned} H_3 &= \sum\sum (d^1_{\zeta_0} + d^2_{\zeta_3}) + \sum\sum (d^1_{\zeta_3} + d^2_{\zeta_0}) \\ &+ \sum\sum (d^1_{\zeta_1} + d^2_{\zeta_2}) + \sum\sum (d^1_{\zeta_2} + d^2_{\zeta_1}) \\ &= H^2_3 + H^1_3 + \varphi^2_2 H^1_1 + \varphi^1_1 H^2_2 + \varphi^2_1 H^1_2 + \varphi^1_2 H^2_1, \end{aligned} \tag{47}$$

$$\begin{aligned} H_4 &= \sum\sum (d^1_{\zeta_0} + d^2_{\zeta_4}) + \sum\sum (d^1_{\zeta_4} + d^2_{\zeta_0}) + \sum\sum (d^1_{\zeta_1} + d^2_{\zeta_3}) \\ &+ \sum\sum (d^1_{\zeta_3} + d^2_{\zeta_1}) + \sum\sum (d^1_{\zeta_2} + d^2_{\zeta_2}) \\ &= H^2_4 + H^1_4 + \varphi^2_3 H^1_1 + \varphi^1_3 H^2_1 + \varphi^1_1 H^2_3 + \varphi^2_1 H^1_3 + \varphi^2_2 H^1_2 + \varphi^1_2 H^2_2, \end{aligned} \tag{48}$$

$$\begin{aligned} H_5 &= \sum\sum (d^1_{\zeta_1} + d^2_{\zeta_4}) + \sum\sum (d^1_{\zeta_4} + d^2_{\zeta_1}) \\ &+ \sum\sum (d^1_{\zeta_2} + d^2_{\zeta_3}) + \sum\sum (d^1_{\zeta_3} + d^2_{\zeta_2}) \\ &= \varphi^2_4 H^1_1 + \varphi^1_1 H^2_4 + \varphi^2_1 H^1_4 + \varphi^1_4 H^2_1 + \\ &\varphi^2_3 H^1_2 + \varphi^1_2 H^2_3 + \varphi^2_2 H^1_3 + \varphi^1_3 H^2_2, \end{aligned} \tag{49}$$

$$\begin{aligned} H_6 &= \sum\sum (d^1_{\zeta_2} + d^2_{\zeta_4}) + \sum\sum (d^1_{\zeta_4} + d^2_{\zeta_2}) + \sum\sum (d^1_{\zeta_3} + d^2_{\zeta_3}) \\ &= \varphi^2_4 H^1_2 + \varphi^1_2 H^2_4 + \varphi^2_2 H^1_4 + \varphi^1_4 H^2_2 + \varphi^2_3 H^1_3 + \varphi^1_3 H^2_3, \end{aligned} \tag{50}$$

$$\begin{aligned} H_7 &= \sum\sum (d^1_{\zeta_3} + d^2_{\zeta_4}) + \sum\sum (d^1_{\zeta_4} + d^2_{\zeta_3}) \\ &= \varphi^2_4 H^1_3 + \varphi^1_3 H^2_4 + \varphi^2_3 H^1_4 + \varphi^1_4 H^2_3, \end{aligned} \tag{51}$$

$$H_8 = \sum\sum (d^1_{\zeta_4} + d^2_{\zeta_4}) = \varphi^2_4 H^1_4 + \varphi^1_4 H^2_4 = 4. \tag{52}$$

Since we have

$$\begin{aligned} H_{\text{all}} &= H_1 + H_2 + H_3 + H_4 + H_5 + H_6 + H_7 + H_8 \\ &= \sum_{b=1}^{2(B_1+B_2)+4} C^b_{2(B_1+B_2)+4} b, \end{aligned} \tag{53}$$

which can be seen in Proof 2 in the Appendix, the ABEP of the G-QSM for $L = 2$ is given by

$$P_b^{L=2} = D(\bar{\varsigma}_1)F(\bar{\varsigma}_1) + D(\bar{\varsigma}_2)F(\bar{\varsigma}_2) + \cdots + D(\bar{\varsigma}_8)F(\bar{\varsigma}_8), \tag{54}$$

where $D(\bar{\varsigma}_m) = H_m/R$ and can be obtained from (45)-(52).

ABEP of G-QSM for $L > 2$

For case of $L > 2$, we denote the two different G-QSM symbols by $\mathbf{x}^i$ and $\mathbf{x}^j$:

$$\mathbf{x}^i = \begin{bmatrix} \mathbf{x}^i_1 \\ \vdots \\ \mathbf{x}^i_L \end{bmatrix}, \mathbf{x}^j = \begin{bmatrix} \mathbf{x}^j_1 \\ \vdots \\ \mathbf{x}^j_L \end{bmatrix}. \tag{55}$$

Algorithm 1 ABEP of the proposed G-QSM system with $L > 2$

Input: $R = \sum_{l=1}^{L} 2B_l + 2$, $\varphi^l_{n_l}$, $l = (1, 2, ..., L), n_l = (0, 1, 2, 3, 4)$, $t = 0$, $P_b^{L>2} = 0$;
Output: $P_b^{L>2}$;

```
for n_1 ∈ (0,4) do
    χ_1 = n_1;
    for n_2 ∈ (0,4) do
        χ_2 = n_2;
        ...
        for n_L ∈ (0,4) do
            χ_L = n_L;
            t = t + 1;
            χ = χ_1 + χ_2 + ... + χ_L;
            ς̄ = χ/2σ^2;
            H_(n_1,...,n_l) = Σ Σ ··· Σ (d^1_{ς n_1} + d^2_{ς n_2} + ··· d^L_{ς n_L});
            P_b^{L>2} = P_b^{L>2} + H_(n_1,...,n_l) F(ς̄);
        end for
        ...
    end for
end for
P_b^{L>2} = P_b^{L>2}/R.
```

Then the ED between them can be expressed as

$$\chi = \|\mathbf{x}^i - \mathbf{x}^j\|^2 = \sum_{l=1}^{L} \|\mathbf{x}^i_l - \mathbf{x}^j_l\|^2 = \sum_{l=1}^{L} \chi_l, \tag{56}$$

where $\chi_l = \|\mathbf{x}^i_l - \mathbf{x}^j_l\|^2 = n_l$. The HD between $\mathbf{x}^i$ and $\mathbf{x}^j$ is:

$$d_\varsigma = \sum_{l=1}^{L} d^l_\varsigma, \tag{57}$$

where d^l_ς denotes the HD between $\mathbf{x}^i_l$ and $\mathbf{x}^j_l$.

According to (23) and (56), there are only $4L$ different values. For each combination $(n_1, n_2, ..., n_L)$, $n_l = (0, 1, 2, 3, 4)$, we have $\chi = n_1 + n_2 + ... + n_L$ and the corresponding total HD is given by

$$\begin{aligned} H_{(n_1,...,n_L)} &= \sum\sum \cdots \sum (d^1_{\varsigma n_1} + d^2_{\varsigma n_2} + \cdots d^L_{\varsigma n_L}) \\ &= \prod_{v=2}^{L} \varphi^v_{n_v} \sum d^1_{\varsigma n_1} + \prod_{v=1, v\neq 2}^{L} \varphi^v_{n_v} \sum d^2_{\varsigma n_2} + \\ &\quad \prod_{v=1, v\neq 3}^{L} \varphi^v_{n_v} \sum d^3_{\varsigma n_3} + \cdots \prod_{v=1, v\neq L}^{L} \varphi^v_{n_v} \sum d^L_{\varsigma n_L} \\ &= \prod_{v=2}^{L} \varphi^v_{n_v} H^1_{n_1} + \prod_{v=1, v\neq 2}^{L} \varphi^v_{n_v} H^2_{n_2} + \\ &\quad \prod_{v=1, v\neq 3}^{L} \varphi^v_{n_v} H^3_{n_3} + \cdots \prod_{v=1, v\neq L}^{L} \varphi^v_{n_v} H^L_{n_L}. \end{aligned} \tag{58}$$

where H^l_n and φ^l_n can be obtained by (41) and (42), respectively. Since $\sum_{n_1=0}^{4} \cdots \sum_{n_L=0}^{4} H_{(n_1,\cdot,n_L)} = \sum_{r=1}^{R} C^r_R r$ (which can be seen in Proof 3 of the Appendix), the ABEP calculation of $P_b^{L>2}$ can be described in Algorithm 1.

Algorithm 2 The proposed M-OMP detector for the G-QSM system

Input: $\hat{\mathbf{y}}$, $\hat{\mathbf{H}}$, m, $\Lambda_0=\phi$, N_Q^l $(l=1,...,L)$, $\lambda_0=\phi$, $\mathbf{r}_0=\hat{\mathbf{y}}$, flag=0,$\mathbb{I}=\phi$,$\mathbb{S}=\phi$

Output: $(l_{\Re}^1,...,l_{\Re}^L,l_{\Im}^1,...,l_{\Im}^L)$, $(x_{\Re}^1,...,x_{\Re}^L,x_{\Im}^1,...,x_{\Im}^L)$.

$\mathbf{l}_1=\arg\mathrm{sort}(|\mathbf{H}^H\mathbf{r}_0|)$;
$\mathbf{l}_1^m=\mathbf{l}_1(1:m)$
for $t_1\in(1,m)$ **do**
  $l_{t_1}=\mathbf{l}_1^m(t_1)$
  $\Lambda_1=[l_{t_1}]$;
  $\tilde{\mathbf{s}}_1=\mathbb{D}((\mathbf{H}_{\Lambda_1}^H\mathbf{H}_{\Lambda_1})^{-1}\mathbf{H}_{\Lambda_1}^H\mathbf{y})$;
  $\mathbf{r}_1=\mathbf{y}-\mathbf{H}_{\Lambda_1}\tilde{\mathbf{s}}_1$;
  Get the QSM symbol index T_1 including all the indices of the t_1-th QSM symbol;
  $\mathbf{l}_2=\arg\mathrm{sort}(|\mathbf{H}^H\mathbf{r}_1|)$;
  $\mathbf{l}_2=\mathrm{setdiff}(\mathbf{l}_2,T_1)$;
  $\mathbf{l}_2^m=\mathbf{l}_2(1:m)$
  for $t_2\in(1,m)$ **do**
    $l_{t_2}=\mathbf{l}_2^m(t_2)$
    $\Lambda_2=[l_{t_1};l_{t_2}]$;
    $\tilde{\mathbf{s}}_2=\mathbb{D}((\mathbf{H}_{\Lambda_2}^H\mathbf{H}_{\Lambda_2})^{-1}\mathbf{H}_{\Lambda_2}^H\mathbf{y})$;
    $\mathbf{r}_2=\mathbf{y}-\mathbf{H}_{\Lambda_2}\tilde{\mathbf{s}}_2$;
    Get the QSM symbol indices T_2 including all the indices of the t_1-th and t_2-th QSM symbols;
    $\mathbf{l}_3=\arg\mathrm{sort}(|\mathbf{H}^H\mathbf{r}_2|)$;
    $\mathbf{l}_3=\mathrm{setdiff}(\mathbf{l}_3,T_2)$;
    $\mathbf{l}_3^m=\mathbf{l}_3(1:m)$
    $\cdots$
    for $t_{2L}\in(1,m)$ **do**
      $l_{t_{2L}}=\mathbf{l}_L^m(t_{2L})$
      $\Lambda_{2L}=[l_{t_1},l_{t_2},...,l_{t_{2L}}]$;
      $\tilde{\mathbf{s}}_{2L}=\mathbb{D}((\mathbf{H}_{\Lambda_{2L}}^H\mathbf{H}_{\Lambda_{2L}})^{-1}\mathbf{H}_{\Lambda_{2L}}^H\mathbf{y})$
      $\mathbb{I}=[\mathbb{I};\Lambda_{2L}]$;$\mathbb{S}=[\mathbb{S};\tilde{\mathbf{s}}_{2L}]$;
      $flag=flag+1$;
      if $\left\|\hat{\mathbf{y}}-\hat{\mathbf{H}}_{\Lambda_{2L}}\tilde{\mathbf{s}}_{2L}\right\|_F^2\leqslant V_{\mathrm{th}}$ **then**
        $(l_{\Re}^1,...,l_{\Re}^L,l_{\Im}^1,...,l_{\Im}^L)=\Lambda_{2L}$,
        $(x_{\Re}^1,...,x_{\Re}^L,x_{\Im}^1,...,x_{\Im}^L)=\tilde{\mathbf{s}}_{2L}$;
        return;
      else
        $Dist(flag)=\left\|\hat{\mathbf{y}}-\hat{\mathbf{H}}_{\Lambda_{2L}}\tilde{\mathbf{s}}_{2L}\right\|^2$;
      end if
    end for
  end for
end for
$[L_{min},s_{min}]=min(Dist)$.
$(l_{\Re}^1,...,l_{\Re}^L,l_{\Im}^1,...,l_{\Im}^L)=\mathbb{I}_{L_{min}}$,
$(x_{\Re}^1,...,x_{\Re}^L,x_{\Im}^1,...,x_{\Im}^L)=\mathbb{S}_{L_{min}}$;

Compressive Sensing Detector for the Proposed G-QSM System

Proposed EM-OMP detector

In order to reduce the complexity of the ML detector, in this section CS aided detection is investigated in the context of our proposed G-QSM system. Firstly, the received signal of Eq. (2) is rewritten in the real-valued form as

$$\underbrace{\begin{bmatrix}\Re(\mathbf{y})\\ \Im(\mathbf{y})\end{bmatrix}}_{\hat{\mathbf{y}}}=\underbrace{\begin{bmatrix}\Re(\mathbf{H}) & -\Im(\mathbf{H})\\ \Im(\mathbf{H}) & \Re(\mathbf{H})\end{bmatrix}}_{\hat{\mathbf{H}}}\underbrace{\begin{bmatrix}\Re(\mathbf{x})\\ \Im(\mathbf{x})\end{bmatrix}}_{\hat{\mathbf{x}}}+\underbrace{\begin{bmatrix}\Re(\mathbf{n})\\ \Im(\mathbf{n})\end{bmatrix}}_{\hat{\mathbf{n}}}, \tag{59}$$

where $\hat{\mathbf{y}}\in\Re^{2N_r\times1}$,$\mathbf{H}\in\Re^{2N_r\times2N_t}$, $\hat{\mathbf{x}}\in\Re^{2N_t\times1}$ and $\hat{\mathbf{n}}\in\Re^{2N_r\times1}$. Therefore, the sparsity of $\hat{\mathbf{x}}$ is determined by $2L$, and the indices of the nonzero elements are distributed rather specifically, because the activated TA indices conveying real-valued APM symbols are located at $(1,...N_Q^1),...,(\sum_{i=1}^{L-1}N_Q^i+1,...,N_t)$ in the sequence, while the activated TA indices conveying the imaginary APM symbols are located at $(N_t+1,...N_t+N_Q^1),...,(\sum_{i=1}^{L-1}N_Q^i+N_t+1,...,2N_t)$ in the sequence. This fact can be beneficially exploited for CS detection.

In the G-QSM detection, the key issue is that of estimating the accurate activated indices by our CS algorithm. In our proposed EM-OMP algorithm, the Multipath Matching Pursuit (MMP) algorithm of [37] is invoked for the detection of the activated indices, which are introduced as follows.

Step 1: Estimate the first activated index as

$$\mathbf{l}_1=\arg\mathrm{sort}(|\mathbf{H}^H\mathbf{r}_0|). \tag{60}$$

Then we get the m candidates as $\mathbf{l}_1^m=\mathbf{l}_1(1:m)$.

Step 2: Estimate the second activated index. For the t_1-th candidate in $\mathbf{l}_1^m$, m candidates are estimated as

$$\mathbf{l}_2=\arg\mathrm{sort}(|\mathbf{H}^H\mathbf{r}_1|),\mathbf{l}_2^m=\mathbf{l}_2(1:m), \tag{61}$$

where $\mathbf{r}_1=\mathbf{y}-\mathbf{H}_{\Lambda_1}\tilde{\mathbf{s}}_1$ with $\Lambda_1=[l_{t_1}]$ and $\tilde{\mathbf{s}}_1=\mathbb{D}((\mathbf{H}_{\Lambda_1}^H\mathbf{H}_{\Lambda_1})^{-1}\mathbf{H}_{\Lambda_1}^H\mathbf{y})$.

Step 3: Repeat Step 2, until we get the $2L$-th activated index. As a result, there may be m^{2L} possible index combinations. Since the locations of the activated indices are restricted, the estimated candidate indices in each step are from different level. Considering $N_t=4$, $L=2$, $m=2$ and $\mathbf{l}_1^m=(1,4)$ for example, if $\mathbf{l}_2=(2,3,4,5,1,6,7,8)$ is estimated in Step 2 based on the index '1', then we have $\mathbf{l}_2^m=(3,4)$; If we get $\mathbf{l}_2=(5,4,1,2,3,4,6,7,8)$ based on the index $'4'$, we have $\mathbf{l}_2^m=(1,2)$. Then we arrive at the following 4 index combinations $\{(1,3),(1,4),(4,1),(4,2)\}$. Finally, we remove the identical combinations and arrive at the final index combinations of $\{(1,3),(1,4),(2,4)\}$.

Step 4: Obtain the accurate one from the m^{2L} possible candidates. For each combination $\Lambda_{2L}=[l_{t_1},l_{t_2},...,l_{t_{2L}}]$, the corresponding symbol vector is estimated as $\tilde{\mathbf{s}}_{2L}=\mathbb{D}((\mathbf{H}_{\Lambda_{2L}}^H\mathbf{H}_{\Lambda_{2L}})^{-1}\mathbf{H}_{\Lambda_{2L}}^H\mathbf{y})$. If $(\Lambda_{2L},\tilde{\mathbf{s}}_{2L})$ satisfies

$$\left\|\hat{\mathbf{y}}-\hat{\mathbf{H}}_{\Lambda_{2L}}\tilde{\mathbf{s}}_{2L}\right\|_F^2\leqslant V_{\mathrm{th}}, \tag{62}$$

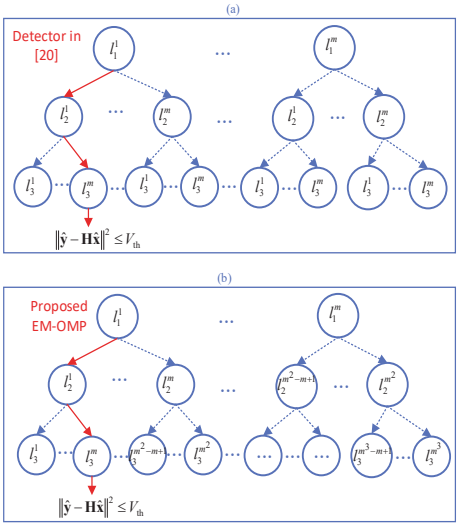

Fig. 4. Differences between the proposed EM-OMP detector and the detector in [20] at $L = 3$.

where $V_{\text{th}} = \beta N_r \sigma^2$ is a threshold defined in [36], $(\Lambda_{2L}, \tilde{\mathbf{s}}_{2L})$ is taken as the final result; Otherwise, the specific combination associated with the smallest Euclidean distance will be considered as the final result. More specifically, the proposed EM-OMP detector is summarized in Algorithm 2.

Moreover, the difference between the proposed EM-OMP detector and the detector in [20] is shown in Fig. 4, where l_i^j represents the j-th candidate in the i-th step. Observe from Fig. 4 (a) that in [20], $(l_i^1, l_i^2, ..., l_i^m)$ for the $(i-1)$-th candidate are always the same and obtained by (60), while those in the EM-OMP detector may be different. Moreover, $m = N_Q^i$ ordered indices are used for constructing $(\prod_{i=1}^{L} N_Q^i)^2$ legitimate TACs for approaching the optimal performance in [20], while m is a small number in our proposed EM-OMP detector, imposing a reduced complexity.

Complexity Analysis

In this section, the complexity of the proposed EM-OMP detector is analyzed in terms of real-valued Floating point (Flops) operations, including real-valued multiplications and real-valued additions, since according to (56), the proposed EM-OMP detector operates in the real-valued domain. For specific real matrices $A \in {}^{M\times N}, B \in {}^{N\times N}, D \in {}^{M\times 1}$, the complexity of the matrix operations AB, $A^H A$, B^{-1} and $\|D\|_F^2$ are expressed as

$$\begin{aligned} &C_{AB} = MN(N+N-1) \\ &C_{A^H A} = MN^2 + N(M - \tfrac{N}{2}) - \tfrac{N}{2} \\ &C_{B^{-1}} = \tfrac{1}{3}N^3 + \tfrac{2}{3}N \\ &C_{\|D\|^2} = M + M - 1 \end{aligned}. \tag{63}$$

According to (56) and Algorithm 2, the complexity of the proposed EM-OMP detector is expressed as

$$\begin{aligned} C_{\text{Pro}} = N_{avg} \sum_{t=1}^{2L} [&\underbrace{(4N_r^2 + 2N_r)(t-1/2)}_{C_{(\mathbf{H}^H\mathbf{H})}} + \underbrace{(\frac{1}{3}t^3 + \frac{2t}{3})}_{C_{(\cdot)^{-1}}} \\ &+ \underbrace{4N_r t^2 - 2N_r + 4N_r t - t}_{C_{(\cdot\mathbf{H}_{\Lambda_t}\mathbf{y})}} + \underbrace{4N_r t}_{C_{(\mathbf{y}-\mathbf{H}_{\Lambda_t}\mathbf{s}_t)}}] + \underbrace{8N_t N_r}_{C_{(\mathbf{H}^H\mathbf{r}_i)}} \cdot 2L \\ &+ N_{avg} \underbrace{4N_r - 1}_{||\cdot||^2}. \end{aligned} \tag{64}$$

where N_{avg} denotes the average search candidates of the proposed detector.

For comparison, according to [20], the complexity of the ML, of the Bayesain CS (BCS) [35], ECS [20], and of the Compressive Sampling Matching Pursuit (CoSaMP) [34] detectors are expressed as

$$C_{\text{ML}} = (8N_r L + 4N_r - 1)2^R, \tag{65}$$

$$\begin{aligned} C_{\text{ECS}} = \sum_{t=1}^{2L-1} [&\underbrace{(4N_r^2 + 2N_r)(t-1/2)}_{C_{(\mathbf{H}^H\mathbf{H})}} + \underbrace{(\frac{1}{3}t^3 + \frac{2t}{3})}_{C_{(\cdot)^{-1}}} \\ &+ \underbrace{4N_r t^2 - 2N_r + 4N_r t - t}_{C_{(\cdot\mathbf{H}_{\Lambda_t}\mathbf{y})}} + \underbrace{4N_r t}_{C_{(\mathbf{y}-\mathbf{H}_{\Lambda_t}\mathbf{s}_t)}}] + \underbrace{8N_t N_r}_{C_{(\mathbf{H}^H\mathbf{r}_i)}} \cdot 2L + \\ &N_{avg}[\underbrace{(4N_r^2 + 2N_r)(2L-1/2)}_{C_{(\mathbf{H}^H\mathbf{H})}} + \underbrace{(\frac{1}{3}(2L)^3 + \frac{4L}{3})}_{C_{(\cdot)^{-1}}} \\ &+ \underbrace{4N_r(2L)^2 - 2N_r + 4N_r 2L - 2L}_{C_{(\cdot\mathbf{H}_{\Lambda_{2L}}\mathbf{y})}} + \underbrace{4N_r 2L}_{C_{(\mathbf{y}-\mathbf{H}_{\Lambda_{2L}}\mathbf{s}_{2L})}}] \underbrace{4N_r - 1}_{||\cdot||^2}], \end{aligned} \tag{66}$$

$$\begin{aligned} C_{\text{BCS}} = &\underbrace{(4N_r^2 + 2N_r)(2N_t - 1/2)}_{C_{(\mathbf{H}\mathbf{H}^H)}} + 2N_r + \underbrace{(\frac{1}{3}(2N_r)^3 + \frac{4N_r}{3})}_{C_{(\cdot)^{-1}}} \\ &+ 2N_t 4N_r + 2N_t 2N_r(4N_r - 1) + 4N_t, \end{aligned} \tag{67}$$

$$\begin{aligned} C_{\text{Cosamp}} = w_{co}[&\underbrace{(4N_r^2 + 2N_r)(K-1/2)}_{C_{(\mathbf{H}_{\Lambda_t}{}^H\mathbf{H}_{\Lambda_t})}} + \underbrace{(\frac{1}{3}K^3 + \frac{2K}{3})}_{C_{(\cdot)^{-1}}} \\ &+ \underbrace{4N_r K^2 - 2N_r + 4N_r K - K}_{C_{(\cdot\mathbf{H}_{\Lambda_t}\mathbf{y})}} + \underbrace{4N_r K}_{C_{(\mathbf{y}-\mathbf{H}_{\Lambda_t}\mathbf{s}_t)}} + \underbrace{4N_r - 1}_{||\cdot||^2}]. \end{aligned} \tag{68}$$

In a word, the complexity order of these detectors are presented in Table I.

Simulation Results

In this subsection, the performance results of the proposed G-QSM associated with different antenna configurations are presented and compared. In all the simulation results, Rayleigh channel with perfect channel state information is assumed. For simplicity, (N_t, N_r, L, M) represent the antenna setups.

Fig. 5 and Fig . 6 compare the performance of the proposed G-QSM system to that of the SM-VBLAST and VBLAST systems at 12 bpcu and 16 bpcu, respec-

TABLE I
COMPLEXITY ORDER OF DIFFERENT DETECTORS FOR G-QSM SYSTEM

Detector	Complexity order (Flops)
ML	$O(NrL2^R) + O(Nr2^R)$
CoSaMP	$O(N_r^2K) + O(N_rK) + O(K^3)$ $+O(N_rK^2) + O(N_rK) + O(N_r)$
BCS	$O(N_r^3) + O(N_r^2N_t) + O(N_rN_t)$ $+O(N_r)+O(N_t)$
ECS	$O(N_{avg}N_r^2L) + O(N_{avg}L^3) + O(N_{avg}N_rL^2)$ $+O(N_{avg}N_tN_rL) + O(N_{avg}N_r)$
Proposed	$O(N_{avg}N_r^2L) + O(N_{avg}L^3) + O(N_{avg}N_rL^2)$ $+O(N_{avg}N_tN_rL) + O(N_{avg}N_r)$

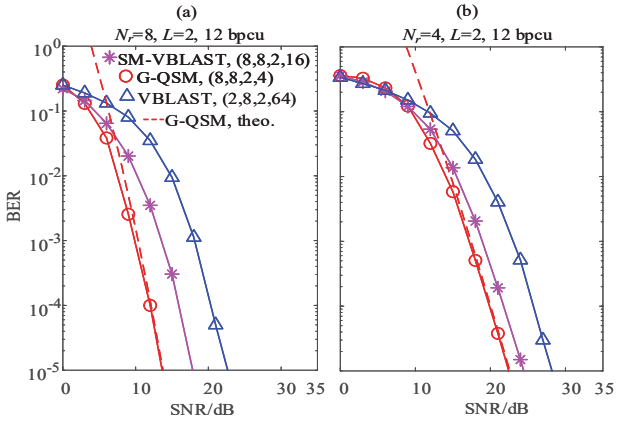

Fig. 5. Performance comparison of the proposed G-QSM system and of the SM-VBLAST and VBLAST systems having $L = 2$ at 12 bpcu; (a) $N_r = 8$; (b) $N_r = 4$.

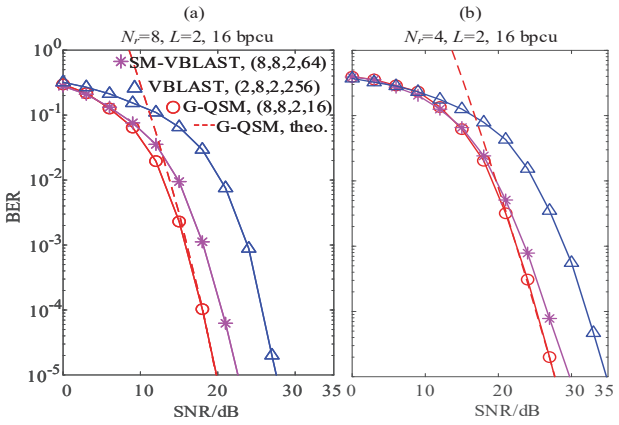

Fig. 6. Performance comparison of the proposed G-QSM system and of the SM-VBLAST and VBLAST systems having $L = 2$ at 16 bpcu; (a) $N_r = 8$; (b) $N_r = 4$.

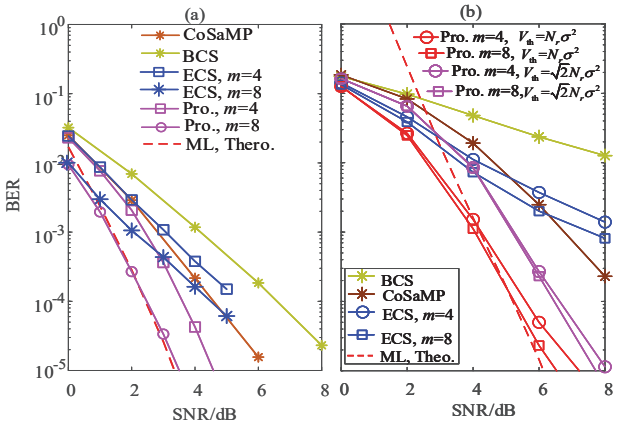

Fig. 7. Performance comparison of the proposed G-QSM system with different detectors. a) $N_t = 128, N_r = 32, L = 1, M = 4$ at 16 bpcu; b)$N_t = 128, N_r = 32, L = 2, M = 4$ at 28 bpcu.

tively[3]. Specifically, in Fig. 5 (a), the parameters of $(8, 8, 2, 4)$, $(8, 8, 2, 16)$ and $(2, 8, 2, 64)$ are employed for the proposed G-QSM system, for SM-VBLAST and for the VBLAST systems to obtain the same normalized throughput of 12 bpcu. In Fig. 5 (b), the parameters of $(8, 4, 2, 4)$, $(8, 4, 2, 16)$ and $(2, 4, 2, 64)$ are employed for the proposed G-QSM, SM-VBLAST and VBLAST systems to obtain the same normalized throughput of 12 bpcu. In Fig. 6 (a), the parameters of $(8, 8, 2, 16)$, $(8, 8, 2, 64)$ and $(2, 8, 2, 256)$ are employed for the proposed G-QSM system, SM-VBLAST and VBLAST systems to obtain the same normalized throughput of 16 bpcu. In Fig. 6 (b), the parameters of $(8, 4, 2, 16)$, $(8, 4, 2, 64)$ and $(2, 4, 2, 256)$ are employed for the proposed G-QSM, SM-VBLAST and VBLAST systems to obtain the same normalized throughput of 16 bpcu. ML detectors are employed in the above-mentioned setups. Moreover, the analytical ABEP performances of the proposed G-QSM system are added as benchmarkers, which become quite accurate upon increasing the SNR values. Observe from Fig. 5 that the proposed G-QSM system using QPSK is capable of providing a 2.5 dB and 7.5 dB gain over the SM-VBLAST and VBLAST systems at BER=10^{-5} for both over-determined and under-determined setups. This trend can also be observed for the G-QSM system using 16-QAM in Fig 6.

Figs. 7-8 compare the performance vs complexity of the different detectors used by the proposed G-QSM system having $N_t = 128, N_r = 32, M = 4$ for different values of L, respectively. In massive MIMO setups, the ML detector becomes impractical, hence only the theoretical curves of the ML detector are added as benchmarkers. Furthermore, $V_{\text{th}} = N_r\sigma^2$ is employed in the proposed EM-OMP detector in Fig. 7 (a) and Fig. 8(a). For the sake of comparing scenarios of similar complexity, the same values of m are selected for the ECS detector of [20]. Since m is much smaller than N_Q^i, the ECS of [20] exhibits an error floor in the high-SNR region. Observe from Fig. 7 that the performance of the proposed EM-OMP detector improves as m increases and it provides significant performance gains over the existing CoSaMP , BCS, ECS detectors at a lower complexity for both of the above-mentioned setups. For the case of $L = 1$, the transmission rate is 16 bpcu, and the complexity of the ML detector is around 2.5×10^7 Flops/bpcu. By contrast, the complexity becomes around 1.7×10^{11} Flops/bpcu for the case of $L = 2$. Observe from Figs. 7-8 that he

[3]Our comparison is limited to V-BLAST and SM-VBLAST associated with the same value of L because (1) they have the same power consumption; (2) they have the same inter-antenna interference; (3) they have the same inter-antenna synchronization complexity.

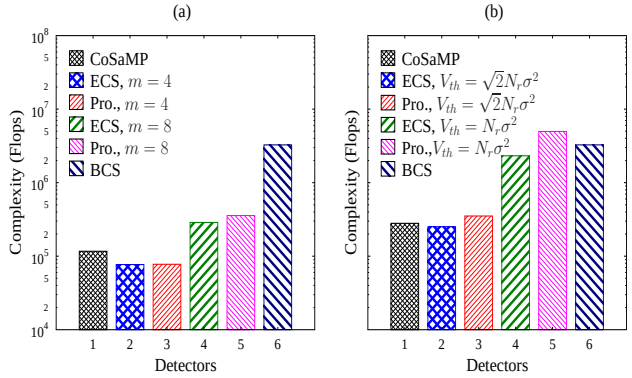

Fig. 8. Complexity comparison of the proposed G-QSM system with different detectors. a) $N_t = 128, N_r = 32, L = 1, M = 4$ at 16 bpcu; b)$N_t = 128, N_r = 32, L = 2, M = 4$ at 28 bpcu.

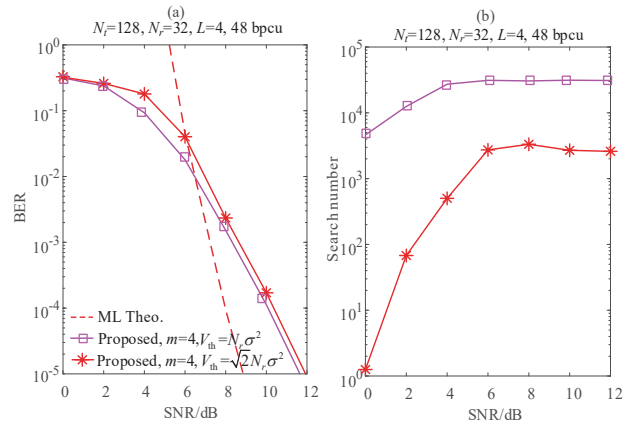

Fig. 9. Performance and complexity comparison of the proposed G-QSM system with different detectors having $N_t = 128, N_r = 32, L = 4, M = 4$ at 48 bpcu.

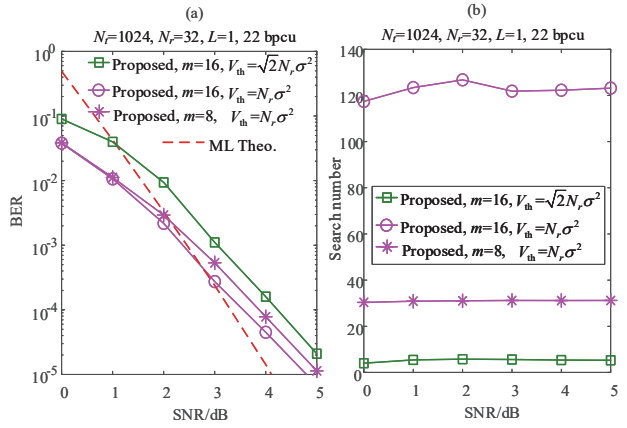

Fig. 10. Performance and complexity comparison of the proposed G-QSM system with different detectors having $N_t = 1024, N_r = 32, L = 1, M = 4$ at 22 bpcu.

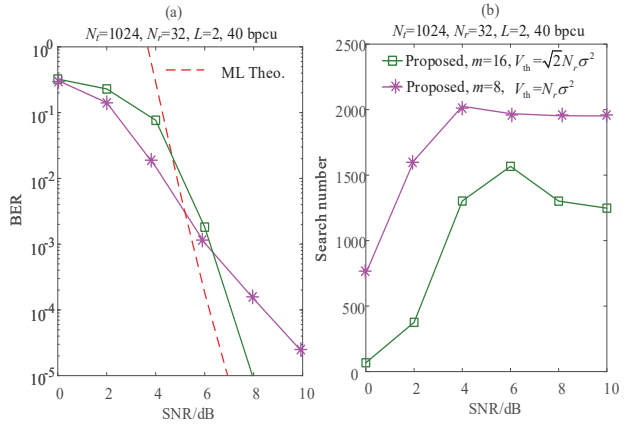

Fig. 11. Performance and complexity comparison of the proposed G-QSM system with different detectors having $N_t = 1024, N_r = 32, L = 2, M = 4$ at 40 bpcu.

proposed EM-OMP detector using $m = 8, V_{\text{th}} = N_r\sigma^2$ is capable of approaching the performance of the ML detector, despite its more than 99% complexity reduction. Furthermore, observe from Figs. 7-8 (b) that the proposed EM-OMP detector using $m = 4, V_{\text{th}} = \sqrt{2}N_r\sigma^2$ is capable of achieving a significant complexity reduction over its counterpart using $m = 4, V_{\text{th}} = N_r\sigma^2$ at a modest performance loss.

Fig. 9 characterizes the performance of the G-QSM system with proposed detector for $N_t = 128, N_r = 32, M = 4, L = 4$. For the case of $L = 4$, the transmission rate is 48 bpcu, where the number of search candidates for the ML detector is 2^{48}. Observe from Fig. 9 that the number of search steps carried out by the proposed EM-OMP detector having $m = 4, V_{\text{th}} = \sqrt{2}N_r\sigma^2$ is reduced to as few as 10^3 from 2^{48} candidates at the cost of around 3 dB performance loss.

In order to provide further insights, Figs. 10-11 compare the performance and complexity of the different detectors for the G-QSM system having $N_t = 1024, N_r = 32, M = 4$ at different values of L. For the case of $L = 1$, the transmission rate is 22 bpcu, while the number of search candidates of the ML detector is 2^{22}. Observe from Fig. 10 that the number of search steps carried out by the proposed EM-OMP detectors having $m = 16, V_{\text{th}} = \sqrt{2}N_r\sigma^2$, $m = 8, V_{\text{th}} = N_r\sigma^2$ and $m = 16, V_{\text{th}} = N_r\sigma^2$ is reduced to as few as 5, 30 and 120 from 2^{22} candidates at the cost of around 1.2 dB, 1 dB, 0.8 dB performance loss. For the case of $L = 2$, the transmission rate is 40 bpcu, while the number of search candidates of the ML detector is 2^{40}. Observe from Fig. 11 that the number of search steps to be carried out by the proposed EM-OMP detectors having $m = 16, V_{\text{th}} = \sqrt{2}N_r\sigma^2$, $m = 8, V_{\text{th}} = N_r\sigma^2$ is reduced to about 10^3 and 2×10^3 from 2^{40} candidates at the cost of around 3 dB and 1 dB performance loss. In conclusion, the proposed EM-OMP detector is eminently suitable for our proposed G-QSM system, since it strikes a compelling performance vs complexity trade-off.

Finally, Fig. 12 compares the performance of the proposed G-QSM system to that of the VBLAST system having the same number of RF chains at high transmission rates. Specifically, $N_t = 128, N_r = 32, L = 1, M = 4$, $N_t = 1024, N_r = 32, L = 1, M = 4$ are employed for the proposed G-QSM system, while $N_t = 2, N_r = 32, L = 2, M = 256$ and $N_t = 2, N_r = 32, L = 2, M = 2048$ are

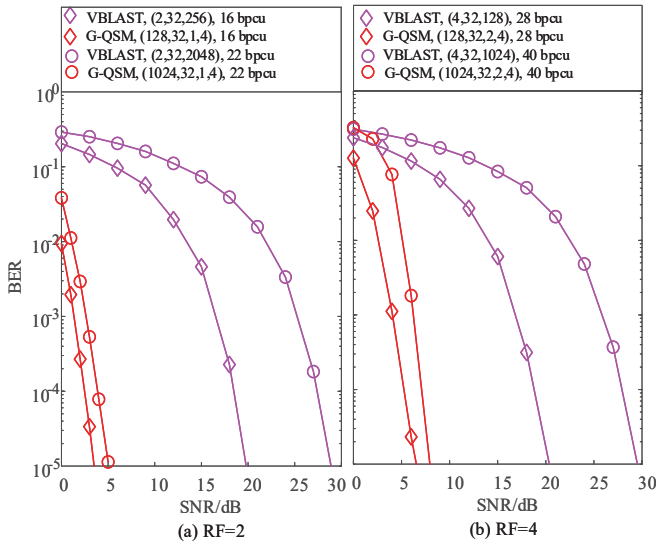

Fig. 12. Performance comparison of the proposed G-QSM system and of the SM-VBLAST and VBLAST systems having the same RF chains and transmission rate; a) RF=2; b) RF=4.

invoked for the VBLAST system to obtain the normalized throughput of 16 bpcu and 22 bpcu having 2 RF chains. Furthermore, $N_t = 128, N_r = 32, L = 2, M = 4$, $N_t = 1024, N_r = 32, L = 2, M = 4$ are employed for the proposed G-QSM system, while $N_t = 4, N_r = 32, L = 4, M = 128$ and $N_t = 4, N_r = 32, L = 4, M = 1024$ are used for the VBLAST system to obtain the normalized throughput of 28 bpcu and 40 bpcu having 4 RF chains. In order to compare systems of the same complexity, the efficient EM-OMP detectors are employed in the proposed G-QSM and MMSE detectors are employed in the VBLAST systems. For the case of 2 RF chains, observe from Fig. 12 (a) that the proposed G-QSM system is capable of outperforming the VBLAST system [4] by 17 dB and 24 dB at 16 bpcu and 22 bpcu respectively at BER=10^{-5} at the cost of an extra channel estimation action, which will be eliminated in our future research by conceiving non-coherent detection at 3 dB performance loss [41]. A similar trend can be observed for the case of 4 RF chains in Fig. 12 (b).

Conclusions

The new low-complexity, high-throughput G-QSM scheme has been proposed. The upper bound of the ABEP of the proposed G-QSM system has also been derived. Furthermore, an efficient CS detector termed as EM-OMP has been proposed for our G-QSM system. Both the theoretical and simulation results have shown that the proposed G-QSM scheme employing a large number of TAs is capable of providing a 20 dB gain over the V-BLAST system having a small identical number of RF chains and the same throughput.

[4]Explicitly, we are not making the unrealistic claim that our scheme outperforms V-BLAST in general, only under the specific assumption of having a rather limited number of RF chains. As the affordable number of RF chains is increased, the throughput becomes quite high, which would necessitate a more advanced CS detector, which will be designed in our future research.

Appendix

Proof 1: $\sum_{b=1}^{B} C_B^b b = B2^{B-1}$.

Specifically, the elements of $C_B^b b$ $b = 1, ..., B$ can be represented in a matrix-form as

$$\{C_B^b b\}_{b=1}^{B} \rightarrow \begin{bmatrix} C_B^1 & & & & & & \\ C_B^2 & C_B^2 & & & & & \\ \vdots & \vdots & \ddots & & & & \\ C_B^b & C_B^b & \cdots & C_B^b & & & \\ \vdots & \vdots & \vdots & \vdots & \ddots & & \\ C_B^{B-1} & C_B^{B-1} & C_B^{B-1} & C_B^{B-1} & \cdots & C_B^{B-1} & \\ C_B^B & C_B^B & C_B^B & C_B^B & C_B^B & \cdots & C_B^B \end{bmatrix}. \tag{69}$$

Then the elements of $2C_B^b b - BC_B^B$ $(b = 1, ..., B)$ can also be represented in a matrix-form as

$$\begin{bmatrix} C_B^1 & C_B^{B-1} & C_B^{B-1} & C_B^{B-1} & C_B^{B-1} & \cdots & C_B^{B-1} \\ C_B^2 & C_B^2 & C_B^{B-2} & C_B^{B-2} & C_B^{B-2} & \cdots & C_B^{B-2} \\ \vdots & \vdots & \ddots & \vdots & \vdots & \vdots & \vdots \\ C_B^b & C_B^b & \cdots & C_B^b & C_B^{B-b} & \cdots & C_B^{B-b} \\ \vdots & \vdots & \vdots & \vdots & \ddots & \vdots & \vdots \\ C_B^{B-1} & C_B^{B-1} & C_B^{B-1} & C_B^{B-1} & \cdots & C_B^{B-1} & C_B^1 \\ C_B^B & C_B^B & C_B^B & C_B^B & C_B^B & \cdots & C_B^B \end{bmatrix}. \tag{70}$$

Since $\sum_{b=1}^{B} C_B^b = 2^B - 1, C_B^b = C_B^{B-b}$, according to (69) and (70), we have

$$2\sum_{b=1}^{B} C_B^b b - C_B^B B = B\sum_{b=1}^{B} C_B^b = B(2^B - 1). \tag{71}$$

Hence, we have $\sum_{b=1}^{B} C_B^b b = B2^{B-1}$.

Proof 2: $H_{\text{all}} = \sum_{t=1}^{8} H_t = \sum_{r=1}^{R} C_R^r r$ with $R = \sum_{l=1}^{2} (2B_l + 2)$. According to (45)-(52), the value of H_{all} can be expressed as

$$\begin{aligned} H_{\text{all}} &= H_1 + H_2 + H_3 + H_4 + H_5 + H_6 + H_7 + H_8 \\ &= (1 + \varphi_1^2 + \varphi_2^2 + \varphi_3^2 + \varphi_4^2)(H_1^1 + H_2^1 + H_3^1 + H_4^1) + \\ &(1 + \varphi_1^1 + \varphi_2^1 + \varphi_3^1 + \varphi_4^1)(H_1^2 + H_2^2 + H_3^2 + H_4^2) \\ &= 2^{2B_2+2}2^{2B_1+1}(2B_1 + 2) + 2^{2B_1+2}2^{2B_2+1}(2B_2 + 2) \\ &= 2^{2B_2+2+2B_1+1}(2B_1 + 2 + 2B_2 + 2) \\ &= \sum_{u=1}^{2(B_1+B_2)+4} C_{2(B_1+B_2)+4}^u u. \end{aligned} \tag{72}$$

Proof 3: $H_{\text{all}} = \sum_{t=1}^{m} H_t = \sum_{r=1}^{R} C_R^r r$ with $R = \sum_{l=1}^{L} (2B_l + 2)$. According to (58), the value of H_{all} can be

expressed as

$$\begin{aligned} H_{\text{all}} &= \sum_{n_1=0}^{4} \cdots \sum_{n_L=0}^{4} H_{(n_1,\ldots,n_L)} \\ &= \sum_{n_1=0}^{4} \cdots \sum_{n_L=0}^{4} [\prod_{v\neq 1} \varphi_{n_v}^{v} H_{n_1}^{1} + \cdots \prod_{v\neq L} \varphi_{n_v}^{v} H_{n_L}^{L}] \\ &= (\sum_{n_2=0}^{4} \cdots \sum_{n_L=0}^{4} \prod_{v=2}^{L} \varphi_{n_v}^{v}) \sum_{n_1=0}^{4} H_{n_1}^{1} + \cdots \\ &+ (\sum_{n_2=0}^{4} \cdots \sum_{n_{(L-1)}=0}^{4} \prod_{v\neq L} \varphi_{n_v}^{v}) \sum_{n_L=0}^{4} H_{n_L}^{L}. \end{aligned} \tag{73}$$

Since we have

$$\begin{aligned} &(\sum_{n_2=0}^{4} \cdots \sum_{n_L=0}^{4} \prod_{v=2}^{L} \varphi_{n_v}^{v}) \sum_{n_1=0}^{4} H_{n_1}^{1} \\ &= (\sum_{n_2=0}^{4} \cdots \sum_{n_{(L-1)}=0}^{4} \prod_{v=2}^{L-1} \varphi_{n_v}^{v}) \sum_{n_L=0}^{4} \varphi_{n_L}^{L} \sum_{n_1=0}^{4} H_{n_1}^{1} \\ &= \sum_{n_2=0}^{4} \varphi_{n_2}^{2} \cdots \sum_{n_{(L-1)}=0}^{4} \varphi_{n_{(L-1)}}^{L-1} \sum_{n_L=0}^{4} \varphi_{n_L}^{L} \sum_{n_1=0}^{4} H_{n_1}^{1} \\ &= 2^{(2B_2+2)} \ldots 2^{(2B_{(L-1)}+2)} 2^{(2B_L+2)} 2^{(2B_1+1)} (2B_1+2) \\ &= 2^{\sum_{l=1}^{L}(2B_l+2)-1} (2B_1+2), \end{aligned} \tag{74}$$

$$\begin{aligned} &(\sum_{n_1=0}^{4} \sum_{n_3=0}^{4} \cdots \sum_{n_L=0}^{4} \prod_{v=1,v\neq 2}^{L} \varphi_{n_v}^{v}) \sum_{n_1=0}^{4} H_{n_2}^{2} \\ &= 2^{\sum_{l=1}^{L}(2B_l+2)-1} (2B_2+2), \\ &\vdots \\ &(\sum_{n_2=0}^{4} \cdots \sum_{n_{(L-1)}=0}^{4} \prod_{v=1,v\neq L}^{L} \varphi_{n_v}^{v}) \sum_{n_L=0}^{4} H_{n_L}^{1} \\ &= 2^{\sum_{l=1}^{L}(2B_l+2)-1} (2B_L+2). \end{aligned} \tag{75}$$

(73) can be finally represented as

$$\begin{aligned} H_{\text{all}} &= \sum_{n_1=0}^{4} \sum_{n_2=0}^{4} \cdots \sum_{n_L=0}^{4} [\sum \sum \cdots \sum (d_{\varsigma n_1}^{1} + d_{\varsigma n_2}^{2} + \cdots d_{\varsigma n_L}^{L})] \\ &= 2^{\sum_{l=1}^{L}(2B_l+2)-1} \sum_{l=1}^{L} (2B_l+2) \\ &= \sum_{r=1}^{R} C_R^r r. \end{aligned} \tag{76}$$

References

[1] M. Di Renzo, H. Haas, A. Ghrayeb, S. Sugiura, and L. Hanzo, "Spatial modulation for generalized MIMO: challenges, opportunities and implementation," *Proceedings of the IEEE*, vol. 102, no. 1, pp. 56-103, Jan. 2014.

[2] P. Yang, Y. Xiao, Y. L. Guan, et al, "Single-carrier spatial modulation: A promising design for large-scale broadband antenna systems," *IEEE Commun. Surveys Tuts.*, vol. 18, no. 3, pp. 1687-1716, Feb. 2016.

[3] A. Chockalingam and B. S. Rajan, Large MIMO Systems. Cambridge, U.K.: Cambridge Univ. Press, 2014.

[4] E. Larsson, O. Edfors, F. Tufvesson, and T. Marzetta, "Massive MIMO for next generation wireless systems," *IEEE Commun. Mag.*, vol. 52, no. 2, pp. 186-195, Feb. 2014.

[5] J. Andrews, S. Buzzi, W. Choi, S. Hanly, A. Lozano, A. Soong, and J. Zhang, "What Will 5G Be?" *IEEE J. Sel. Areas Commun.*, vol. 32,no. 6, pp. 1065-1082, June 2014

[6] A. Adjoudani, E. C. Beck, A. P. Burg, G. M. Djuknic, G. Gvoth, D. Haessig, S. Manji, M. A. Milbrodt, M. Rupp, D. Samardzija, A. B. Siegel, T. Sizer, C. Tran, S. Walker, S. A. Wilkus, P. W. Wolniansky, "Prototype experience for MIMO BLAST over third-generation wireless system," in *IEEE Journal on Selected Areas in Communications*, vol. 21, no. 3, pp. 440-451, 2003.

[7] R. Mesleh, H. Haas, S. Sinanovic, C. W. Ahn, and S. Yun, "Spatial modulation," *IEEE Trans. Veh. Technol.*, vol. 57, no. 4, pp. 2228-2241, Jul. 2008.

[8] P. Yang, M. Di Renzo, Y. Xiao, S. Q. Li and L. Hanzo,"Design guidelines for spatial modulation," *IEEE Commun. Surveys Tuts.*, vol. 17, no. 1, pp. 6-26, First Quart. 2015.

[9] S. Wang, Y. Li, M. Zhao, and J. Wang, "Energy efficient and low-complexity uplink transceiver for massive spatial modulation MIMO," *IEEE Trans. Veh. Technol.*, vol. 64, no. 10, pp. 4617-4632, Oct. 2015.

[10] S. Wang, Y. Li, and J. Wang, "Multiuser detection in massive spatial modulation MIMO with low-resolution ADCs," *IEEE Trans. Wireless Commun.*, vol. 14, no. 4, pp. 2156-2168, Apr. 2015.

[11] L. He, J. Wang, J. Song, and L. Hanzo, "On the multi-user, multi-cell massive spatial modulation uplink: How many antennas for each user?,"*IEEE Trans. Wireless Commun.*, vol. PP, no. 99, pp. 1-1, Dec. 2016.

[12] J. Wang, S. Jia, and J. Song, "Generalised spatial modulation with multiple active transmit antennas and low complexity detection scheme," *IEEE Trans. Wireless Commun.*, vol. 11, no. 4, pp. 1605-1615, Apr. 2012.

[13] T. L. Narasimhan, P. Raviteja and A. Chockalingam"Generalized spatial modulation in large-scale multiuser MIMO systems," *IEEE Trans. Wireless Commun.* vol. 14, no. 7, pp. 1536-1276, March 2015.

[14] P. Patcharamannepakorn, S. Wu, C. Wang, E. M. Aggoune, M. M. Alwakeel, X. Ge, and M. Di. Renzo,"Spectral, energy, and economic efficiency of 5G multicell massive mimo systems with generalized spatial modulation", *IEEE Trans. Veh. Technol.*, vol. 65, no. 12, pp. 9715-9731, Dec., 2016.

[15] N. Ishikawa, R. Rajashekar, S. Sugiura and L. Hanzo, "Generalized spatial modulation based reduced-RF-Chain millimeter-wave communications," *IEEE Trans. Veh. Technol.*, vol. PP, no. 99, pp. 1-1, April, 2016.

[16] C.-C. Cheng, H. Sari, S. Sezginer and Y. Su, "Enhanced spatial modulation with multiple signal constellations,"*IEEE Trans. Commun.*, vol. 63, no. 6, June 2015, pp. 2237-2248.

[17] O. Osman, "Variable active antenna spatial modulation,"*IEEE IET Microwaves, Antennas Propagation* vol. 9, no. 15, pp. 1816-1824 Oct. 2015. 2237-48.

[18] E. Basar, U. Aygolu, E. Panayirci and H. V. Poor, "Space-Time Block Coded Spatial Modulation," *IEEE Trans. Commun.*, vol. 59, no. 3, pp. 823-832, Mar. 2011.

[19] L. Xiao, Y. Xiao, L. You, P. Yang, S. Li and L. Hanzo, "Single-RF and Twin-RF spatial modulation for an arbitrary number of transmit antennas," *IEEE Trans. Veh. Tech.*, vol. pp, no. 12, Dec. 2017.

[20] L. Xiao, Y. Xiao, C. Xu, P. Yang, S. Li and L. Hanzo. Compressive sensing assisted spatial multiplexing aided spatial modulation. *IEEE Trans. Wireless Commun.*, vol. 17, no. 2, Feb. 2018.

[21] R. Mesleh, S. S. Ikki, and H. M. Aggoune, "Quadrature spatial modulation," *IEEE Trans. Veh. Technol.*, vol. 64, no. 6, pp. 2738-2742, June. 2015.

[22] S. Althunibat and R. Mesleh, "Performance analysis of quadrature spatial modulation in two-way relaying cooperative networks," *IET Commun.*, vol. 12, no. 4, pp. 466-472, 2018.

[23] A. Younis, R. Mesleh and H. Haas, "Quadrature spatial modulation performance over Nakagami-m fading channels," *IEEE Trans. Veh. Technol.*, vol. 57, no. 4, pp. 2228-2241, Jul. 2008.

[24] I. A. Nahhal, O. A. Dobre and S. S. Ikki, "Quadrature spatial modulation decoding complexity: study and reduction," *IEEE wireless Commun. Lett.* vol. 6, no. 3, June, 2017.

[25] L. Xiao, P. Yang, S. Fan, S. Li, L. Song, and Y. Xiao, "Low-complexity signal detection for large-scale quadrature spatial modulation systems"*IEEE Comun. Lett.*, vol. PP, no. 99, pp. 1-4, Aug., 2016.

[26] Z. Huang, Z. Gao and L. Sun, "Anti-eavesdropping schemem based on quadrature spatial modulation,"*IEEE Commun. Lett.*, vol. 21, no. 3, pp. 532-535, March, 2017.

[27] R. Mesleh, S. Althunibat and A. Younis,"Differential quadrature spatial modulation,"*IEEE Trans. Commun.*, vol. 65, no. 9, Sep., 2017.
[28] L. Wang, Z. Chen, Z. Gong and M. Wu,"Diversity-achieving quadrature spatial modulation," *IEEE Trans. Veh. Tech.*, vol. 66, no. 12, pp. 10764-10775, Dec. 2017.
[29] J. Li, M. Wen, X. Cheng, Y. Yan, S. Song, and M. H. Lee, "Generalised pre-coding aided quadrature spatial modulation," *IEEE Trans. Veh. Tech.*, vol. 66, no. 2, Feb. 2017.
[30] A. Afana, I. A. Mahady and S. Ikki, "Quadrature spatial modulation in MIMO cognitive radio systems with imperfect channel estimation and limited feedback," *IEEE Trans. Commun.*, vol. 65, no. 3, March, 2017.
[31] A. Younis, N. Abuzgaia, R. Mesleh and H. Hass, "Quadrature spatial modulation for 5G outdoor millimeter-wave communications: Capacity analysis,"*IEEE Trans. Wireless Commun.*, vol. 16, no. 5, May, 2017.
[32] C. Yu, S. Hsieh, H. Liang, C. Lu, W. Chung, S. Kuo and S. Pei, "Compressed sensing detector design for space shift keying in MIMO systems," *IEEE Commun. Lett.*, vol. 16, no. 10, pp. 1556-1559, Oct. 2012.
[33] W. Liu, N. Wang, M. Jin, and H. Xu, "Denoising detection for the generalized spatial modulation system using sparse property," *IEEE Commun. Lett.*, vol. 18, no. 1, pp. 22-25, Jan. 2014.
[34] A. G. Rodriguez and C. Masouros, "Low-complexity compressive sensing detection for spatial modulation in large-scale multiple access channels," *IEEE Trans. Commun.*, vol. 63, no. 7, pp. 2565-2579, July 2015.
[35] C. Yang, P. Cheng, Z. Chen, J. A. Zhang, Y. Xiao abd L. Gui, "Near-ML low-complexity detection for generalized spatial modulation", *IEEE Commun. Lett.*, vol. 20, no. 3, pp. 618-621, Mar. 2016.
[36] L. Xiao, P. Yang, Y. Xiao, S. Fan, M. Di. Renzo, W. Xiang, and S. Li, "Efficient compressive sensing detectors for generalized spatial modulation systems," *IEEE Trans. Veh. Technol.*, vol. 66, no. 2, pp. 1284-1298, 2017.
[37] Z. Gao, L. Dai, Z. Wang, S. Chen and L. Hanzo, "Compressive sensing based multiuser detector for the large-scale SM-MIMO uplink," *IEEE Trans. Veh. Technol.*, vol. 65, no. 10, pp. 8725-8730, 2016.
[38] Z. Gao, L. Dai, C. Qi, C. Yuen and Z. Wang, "Near-optimal signal detetcor based on structured compressive sensing for massive SM-MIMO," *IEEE Trans. Veh. Technol.*, vol. 66, no. 2, pp. 1860-1865, 2017.
[39] Z. Gao, L. Dai, S. Han, C. L, Z. Wang and L. Hanzo, "Compressive sensing techniques for next-generation wireless communications," *IEEE Wireless Commun.*, vol. 25, no. 3, pp. 144-153, 2018.
[40] S. Kwon, J. Wang and B. Shim, "Multipath matching pursuit," *IEEE Trans. Inf. Theroy*, vol. 60, no. 5, pp. 2986-3001, May 2014.
[41] N. Ishikawa, R. Rajashekar, C. Xu, S. Sugiura, and L. Hanzo, "Differential space-time coding dispensing with channel estimation approaches the performance of its coherent counterpart in the open-loop massive MIMO-OFDM downlink,"*IEEE Trans. Commun.*, vol. 66, no. 12, pp. 6190-6204, August 2018.

Lixia Xiao received the B.E., M.E., and Ph. D degrees in 2010, 2013 and 2017, respectively from University of Electronic Science and Technology of China (UESTC). Currently, she is a research fellow with the department of Electrical Electronic Engineering of University of Surrey. Her research is in the field of wireless communications and communication theory. In particular, she is very interested in signal detection and performance analysis of wireless communication systems.

Pei Xiao (SM'11) is a professor of Wireless Communications at the Institute for Communication Systems, home of 5G Innovation Centre (5GIC) at the University of Surrey. He is the technical manager of 5GIC, leading the research team at on the new physical layer work area, and coordinating/supervising research activities across all the work areas within 5GIC (www.surrey.ac.uk/5gic research). Prior to this, he worked at Newcastle University and QueenâĂŹs University Belfast. He also held positions at Nokia Networks in Finland. He has published extensively in the fields of communication theory and signal processing for wireless communications.

Yue Xiao (M'04') received the Ph.D degree in communication and information systems from the University of Electronic Science and Technology of China (UESTC) in 2007. He is currently a Professor with National Key Laboratory of Science and Technology on Communications, UESTC. He has published more than 100 international journals and has been in charge of more than 20 projects in the area of Chinese 3G/4G/5G wireless communication systems. He is an inventor of more than 50 Chinese and PCT patents on wireless systems. His research interests are in system design and signal processing toward future wireless communication systems. He currently serves as an Associate Editor of IEEE COMMUNICATIONS LETTERS.

Harald Haas received the PhD degree from the University of Edinburgh in 2001. He currently holds the Chair of Mobile Communications at the University of Edinburgh, and is the founder and Chief Scientific Officer of pureLiFi Ltd as well as the Director of the LiFi Research and Development Center at the University of Edinburgh. His main research interests are in LiFi and visible light communications. He first introduced and coined 'spatial modulation' and 'LiFi'. The latter was listed among the 50 best inventions in TIME Magazine 2011. Prof. Haas was an invited speaker at TED Global 2011, and his talk: "Wireless Data from Every Light Bulb" has been watched online more than 2.5 million times. He gave a second TED Global lecture in 2015 on the use of solar cells as LiFi data detectors and energy harvesters. This has been viewed online more than 2 million times. He has published more than 400 conference and journal papers including a paper in Science. Prof. Haas is editor of IEEE Transactions on Communications and IEEE Journal of Lightwave Technologies. He was co-recipient of recent best paper awards at VTC-Fall, 2013, VTC-Spring 2015, ICC 2016 and ICC 2017. He was co-recipient of the EURASIP Best Paper Award for the Journal on Wireless Communications and Networking in 2015, and co-recipient of the Jack Neubauer Memorial Award of the IEEE Vehicular Technology Society. In 2012 and 2017, he was the recipient of the prestigious Established Career Fellowship from the EPSRC (Engineering and Physical Sciences Research Council) within Information and Communications Technology in the UK. In 2014, he was selected by EPSRC as one of ten RISE (Recognising Inspirational Scientists and Engineers) Leaders in the UK. In 2016, he received the outstanding achievement award from the International Solid State Lighting Alliance. He was elected a Fellow of the Royal Society of Edinburgh in 2017, and was elevated to Fellow of the IEEE in 2017.

Lajos Hanzo (http://www-mobile.ecs.soton.ac.uk) FREng, F'04, FIET, Fellow of EURASIP, received his 5-year degree in electronics in 1976 and his doctorate in 1983 from the Technical University of Budapest. In 2009 he was awarded an honorary doctorate by the Technical University of Budapest and in 2015 by the University of Edinburgh. In 2016 he was admitted to the Hungarian Academy of Science. During his 40-year career in telecommunications he has held various research and academic posts in Hungary, Germany and the UK. Since 1986 he has been with the School of Electronics and Computer Science, University of Southampton, UK, where he holds the chair in telecommunications. He has successfully supervised 119 PhD students, co-authored 18 John Wiley/IEEE Press books on mobile radio communications totalling in excess of 10 000 pages, published 1800+ research contributions at IEEE Xplore, acted both as TPC and General Chair of IEEE conferences, presented keynote lectures and has been awarded a number of distinctions. Currently he is directing a 60-strong academic research team, working on a range of research projects in the field of wireless multimedia communications sponsored by industry, the Engineering and Physical Sciences Research Council (EPSRC) UK, the European Research Council's Advanced Fellow Grant and the Royal Society's Wolfson Research Merit Award. He is an enthusiastic supporter of industrial and academic liaison and he offers a range of industrial courses. He is also a Governor of the IEEE ComSoc and VTS. He is a former Editor-in-Chief of the IEEE Press and a former Chaired Professor also at Tsinghua University, Beijing. For further information on research in progress and associated publications please refer to http://www-mobile.ecs.soton.ac.uk

Abdelrahim Mohamed (S'15-M'16) received the B.Sc. degree (First Class) in electrical and electronics engineering from the University of Khartoum, Sudan, in 2011, the M.Sc. degree (distinction) in mobile and satellite communications, and the Ph.D. degree in electronics engineering from the University of Surrey, U.K., in 2013 and 2016 respectively. He is currently a Postdoctoral Research Fellow with the 5G Innovation Centre (5GIC), U.K. He is currently involved in the RRM, MAC and RAN Management work area, and the New Physical Layer work area in the 5GIC. He was involved in the Energy Proportional eNodeB for LTE-Advanced and Beyond Project, the Planning Tool for 5G Network in mm-wave Band, in parallel to working on the development of the 5G System Level Simulator. His main areas of research interest include radio access network design, system-level analysis, mobility management, energy efficiency and cognitive radio. He secured first place and top ranked in the Electrical and Electronic Engineering Department, University of Surrey, U.K. during his M.Sc. studies. He was a recipient of the Sentinels of Science 2016 Award.